を小児科，眼科，皮膚科の共同で，長期にわたって行う[1]．

1）皮　　膚

多くの例で，port-wine stain に対してレーザー治療(主にパルス色素レーザー療法)を乳幼児期から開始する．

2）眼

緑内障の診断・治療を乳児期から開始する．β遮断薬，アドレナリン作動薬，炭酸脱水素酵素阻害薬の点眼，線維柱帯切除術(trabeculectomy)，隅角切開術(goniotomy)などの手術が行われる．

3）神　　経

てんかん発作の予防・治療が多くの場合，中心となる．第一選択はカルバマゼピン，レベチラセタムなど，第二選択はその他の多くの(より強い効果の期待される)抗てんかん薬である．薬物治療に抵抗性のてんかんが少なくなく，このようなとき外科的治療が考慮される．手術には大脳切除術(半球，脳葉ないし局所切除)，離断術(半球離断など)，迷走神経刺激が含まれる．手術(特に前二者)は手術時年齢が若いほど，半球切除を行ったほど，術後の予後(てんかん発作に関する)は良いとする報告がある．手術を早期に施行することが術後の知能発達を改善するか否かについて決定的なエビデンスはないが，手術の遅れが発達の遅れにつながる可能性は十分考えられる[7]．切除術，離断術の対象とならない難治例の一部に対しては，ケトン食(Atkins 食など)も試みられる．

頭痛は多くの場合片頭痛であり，一般的な片頭痛の予防・治療(イブプロフェン，トリプタンほか)が準用される．近年，脳卒中様エピソードの予防として，あるいは脳静脈血流うっ滞の改善を期待して抗血小板薬の少量(アスピリン 3-5 mg/kg/日)投与が行われるようになった．しかし高レベルのエビデンスはいまだない．

知的障害に関する指導・助言，家庭や教育の環境改善に向けた取り組みを行う．しばしば合併する注意欠陥・多動性障害に対して薬物療法を行う例もある．

Sturge-Weber 症候群の経過と予後は，症例により大きく異なる．重症度もほぼ正常から重度の知能・運動障害まで様々である．脳病変の範囲が広いほど神経症状が重症となりやすい傾向はあるものの，画像所見から臨床的重症度や予後を正確に予測することはできない．

文　　献

1) Thomas-Sohl KA, et al: Sturge-Weber syndrome: a review. Pediatr Neurol 30: 303-310, 2004.
2) 竹下研三ほか：1974 年から 1983 年迄の鳥取県における先天異常調査．先天異常 24: 395-402, 1984.
3) Shirley MD, et al: Sturge-Weber syndrome and port-wine stains caused by somatic mutation in *GNAQ*. N Engl J Med 368: 1971-1979, 2013.
4) Tallman B, et al: Location of port-wine stains and the likelihood of ophthalmic and/or central nervous system complications. Pediatrics 87: 323-327, 1991.
5) 糸数直哉：Sturge-Weber 症候群．小児の診断治療指針第 4 版(「小児内科」「小児外科」編集委員会共編)，p 690-691，東京医学社，2012.
6) 新島新一ほか：Sturge-Weber 症候群．小児中枢神経疾患の画像診断 2008(「小児内科」「小児外科」編集委員会共編)，p 262-266，東京医学社，2007.
7) Bourgeois M, et al: Surgical treatment of epilepsy in Sturge-Weeber syndrome in children. J Neurosurg 106(1 Suppl): 20-28, 2007.

Establishment of *Tsc2*-deficient rat embryonic stem cells

YOSHITAKA ITO[1,2*], HARUNA KAWANO[2,3*], FUMIO KANAI[4], ERI NAKAMURA[4], NORIHIRO TADA[4], SETSUO TAKAI[5], SHIGEO HORIE[3], HAJIME ARAI[1], TOSHIYUKI KOBAYASHI[2] and OKIO HINO[2]

Departments of [1]Neurosurgery, [2]Molecular Pathogenesis and [3]Urology, [4]Laboratory of Genome Research, Research Institute for Diseases of Old Age, Juntendo University Graduate School of Medicine, Tokyo; [5]Department of Clinical Radiology, Faculty of Health Sciences, Hiroshima International University, Hiroshima, Japan

Received December 25, 2014; Accepted February 9, 2015

DOI: 10.3892/ijo.2015.2913

Abstract. Tuberous sclerosis complex (TSC) is an autosomal dominant disorder caused by *TSC1* or *TSC2* mutations. TSC causes the development of tumors in various organs such as the brain, skin, kidney, lung, and heart. The protein complex TSC1/2 has been reported to have an inhibitory function on mammalian target of rapamycin complex 1 (mTORC1). Treatment with mammalian target of rapamycin (mTOR) inhibitors has demonstrated tumor-reducing effects in patients with TSC but is also associated with various adverse effects. In recent years, experiments involving *in vivo* differentiation of pluripotent stem cells have been reported as useful in elucidating mechanisms of pathogenesis and discovering new therapeutic targets for several diseases. To reveal the molecular basis of the pathogenesis caused by the *Tsc2* mutation, we derived embryonic stem cells (ESCs) from Eker rats, which have the *Tsc2* mutation and develop brain lesions and renal tumors. Although several studies have reported the necessity of *Tsc1* and *Tsc2* regulation to maintain ESCs and hematopoietic stem cells, we successfully established not only $Tsc2^{+/+}$ and $Tsc2^{+/-}$ ESCs but also $Tsc2^{-/-}$ ESCs. We confirmed that these cells express pluripotency markers and retain the ability to differentiate into all three germ layers. Comprehensive gene expression analysis of $Tsc2^{+/+}$ and $Tsc2^{+/-}$ ESCs revealed similar profiles, whereas the profile of $Tsc2^{-/-}$ ESCs was distinct from these two. *In vitro* differentiation experiments using these ESCs combined with *in vivo* experiments may reveal the mechanism of the tissue-specific pathogenesis caused by the *Tsc2* mutation and identify specific new therapeutic targets.

Correspondence to: Dr Okio Hino or Dr Toshiyuki Kobayashi, Department of Molecular Pathogenesis, Juntendo University Graduate School of Medicine, 2-1-1 Hongo, Bunkyo-ku, Tokyo 113-8421, Japan
E-mail: ohino@juntendo.ac.jp
E-mail: koba396@juntendo.ac.jp

*Contributed equally

Key words: *Tsc2*, tuberous sclerosis, Eker rat, embryonic stem cell, mTORC1, differentiation

Introduction

Tuberous sclerosis complex (TSC) is a genetic disorder characterized by multisystem involvement and wide phenotypic variability. This condition results in the development of non-cancerous tumors in various organs and most frequently affects the brain, skin, kidney, lung, heart, and retina. TSC manifestations in the central nervous system include cortical tubers, subependymal nodules, subependymal giant cell astrocytomas, and scattered abnormal cells throughout the brain (1). A majority of patients with TSC reveal neurological and/or psychiatric symptoms, including epilepsy, intellectual disability, autism spectrum disorder (ASD), attention deficit, depression, and anxiety disorder, which range from mild to severe and may impair their ability to live an independent life.

Mutation of either *TSC1* or *TSC2* causes TSC (2,3). Protein products of *TSC1* (hamartin) and *TSC2* (tuberin) form a complex that inhibits the Ras homologue enriched in the brain (Rheb), a small G protein that activates mammalian target of rapamycin complex 1 (mTORC1). Defects of *TSC1* or *TSC2* cause excessive mTORC1 activation, which in turn provokes abnormal regulation of important cellular processes such as cellular growth and proliferation (4,5). The Knudson's 'two-hit' model (6) has been the working molecular model for tumor development in TSC for several years. In fact, loss of heterozygosity (LOH) of *TSC1* or *TSC2* has been demonstrated in renal angiomyolipomas (7-9) and in subependymal giant cell astrocytomas (10). However, evidence for LOH in TSC cortical tubers is limited (11). On the other hand, haploinsufficiency of these genes is also speculated to be involved in TSC pathogenesis. To reveal *Tsc* mutation-related mechanisms of the pathogenesis, rodents harboring a defect of the *Tsc1* or *Tsc2* gene have been extensively investigated (12-15). For instance, $Tsc1^{+/-}$ and $Tsc2^{+/-}$ mouse models exhibit learning and memory deficits (16,17). Eker rats are heterozygous for a mutation of *Tsc2* and develop hereditary kidney cancer by the age of 1 year (18-20). Although kidney cancer is rare in human patients with TSC, it is the only cancer known to occur at an increased incidence in TSC. The embryonic lethality of $Tsc2^{-/-}$ Eker rat embryos is characterized by disrupted neuroepithelial growth (21). Although cortical tubers are rare (22), 63% of Eker rats develop brain lesions comprising a mixture of large and elongated cells in both subependymal and subcortical regions (23,24). In contrast, among *Tsc1* and *Tsc2* knock-out

mouse models, only conditional ablation in the brain can induce such lesions (25). Consequently, with regard to brain lesions, the Eker rat model is more similar to the human patients compared with other mouse models.

We observed that the tumorigenicity of *Tsc2*$^{-/-}$ cells derived from mice was effectively inhibited by rapamycin treatment (26). Other groups reported a similar effect when Eker rats or knock-out mice were treated with rapamycin, although some residual tumors were detected (27,28). These findings have provided the rationale for therapy with rapalogues to treat TSC lesions such as lymphangioleiomyomatosis, SEGAs, and angiomyolipomas, directed at the abnormal activation of mTORC1 (29-31). Although decreased tumor volume has been documented, complete cure was not achieved in most cases. In addition, there are several problems associated with long-term use of rapalogues, including various undesirable side-effects. Consequently additional therapeutic molecular targets are required. The pathogenesis of TSC is assumed to be related to abnormal differentiation as a result of *TSC1/2* deficiency. For instance, abnormal giant cells that appear in brain lesions of patients with TSC express both neuronal and glial lineage markers (32). In recent years, a number of articles have revealed differentiation- and cell type-specific abnormalities using *in vitro* differentiation protocols to investigate differentiation of embryonic stem cells (ESCs) and induced pluripotent stem cells (iPSCs). To evaluate roles of *Tsc2* from the viewpoint of differentiation and tissue-specific pathogenesis as well as to compare and combine *in vivo* and *in vitro* models, we established ESCs from Eker rats.

In 2008, authentic rat ESCs were established for the first time (33,34), lagging behind the establishment of mouse (35,36) and human ESCs (37). Using methods described by Buehr *et al* (33), we generated ESCs from blastocysts of Eker rats to establish an *in vivo* experimental system to explore the role of *Tsc2* in TSC pathogenesis. Although several reports have indicated the necessity of *Tsc1* and *Tsc2* regulation to maintain ESCs (38) and somatic stem cells (39) or to establish iPS cells (40), we were able to establish not only *Tsc2*$^{+/+}$ and *Tsc2*$^{+/-}$ ESCs but also *Tsc2*$^{-/-}$ ESCs. To our knowledge, this is the first report describing the generation of *Tsc2*-deficient ESCs.

Materials and methods

Ethics statement. All animal experiments were conducted in strict accordance with the institutional guidelines of Juntendo University for animal experiments. The protocol was approved by the Animal Experimentation Committee of Juntendo University (Tokyo, Japan) (approval no. 250105). All surgical procedures were performed under isoflurane anesthesia, and all efforts were made to minimize animal suffering.

Animals. Genetic homogeneity of Eker rats was maintained in our laboratory by brother-sister mating. Wistar rats, Brown Norway rats, C57BL/6J mice, and nude mice were purchased from Charles River Laboratories Japan, Inc. (Kanagawa, Japan). All animals were housed under specific pathogen-free conditions.

Mouse embryonic fibroblasts (MEFs). MEFs were derived from embryonic day 14.5 C57BL6/J mouse embryos. MEFs were cultured in Knockout DMEM supplemented with 10% fetal bovine serum, 1% L-glutamine, and penicillin streptomycin (all from Gibco Life technologies, Carlsbad, CA, USA) on gelatin-coated dishes. MEFs were treated with mitomycin C (Sigma-Aldrich, St. Louis, MO, USA) for use as feeder cells.

Culture of ESCs. We generated ESCs from Eker rats according to the method reported by Buehr *et al* (33). After double heterozygous mating of Eker rats, E4.5 blastocysts were gently flushed out from uteri using the N2B27 medium (StemCells, Inc., Newark, CA, USA). After removal of zonae pellucidae with acid Tyrode's solution, whole blastocysts were plated and cultured on mitomycin C-treated MEFs in N2B27 medium supplemented with 3 μM of CHIR99021, 1 μM of PD0325901 (both from Axon Medchem BV, Groningen, The Netherlands), 1,000 U/ml rat leukemia inhibitory factor (LIF) (ESGRO®; Millipore, Bedford, MA, USA) [two inhibitors (2i) + LIF condition]. After 5-7 days, blastocyst outgrowths were cut into pieces and replated in the same 2i + LIF medium. Thereafter, emerging ESC colonies were dissociated using Accutase (Innovative Cell Technologies, Inc., San Diego, CA, USA) and passaged every 2-4 days.

Alkaline phosphatase staining. Alkaline phosphatase staining was performed with an alkaline phosphatase kit (85L3R; Sigma-Aldrich) according to the manufacturer's instructions.

Chromosomal analysis. A standard chromosome preparation method using colchicine treatment was employed. Chromosome preparations were analyzed after Giemsa staining. At least 30 metaphase chromosome sets were analyzed for each line.

Genotyping polymerase chain reaction (PCR). Genotyping of ESCs was conducted using PCR on ESC DNA. To discriminate *Tsc2* mutant or wild-type alleles, the following primers were used: 5MFJ (5'-ACC ATC AGG ATG CTG CTG AA-3'), 3MFJ2 (5'-CTA TGG CCA CAT GTG ACC AA-3'), and TSR27 (5'-GCG CCA GAT TCA CCT CAT TA-3') (41). PCR was used to identify the gender of ESCs by amplification of the rat Y chromosome-specific *Sry* gene using the primer pair Sry-F (5'-CAT CGA AGG GTT AAA GTG CCA-3') and Sry-R (5'-ATA GTG TGT AGG TTG TTG TCC-3') (33).

Reverse transcription (RT)-PCR. Total RNA was obtained using a NucleoSpin® RNA II kit (Macherey-Nagel GmbH & Co. KG, Düren, Germany) according to the manufacturer's instructions. Complementary DNA was synthesized using a SuperScript III First-Strand Synthesis SuperMix kit (Invitrogen Life Technologies, Carlsbad, CA, USA) and an oligo-dT primer, according to the manufacturer's instructions. PCR was performed in a thermal cycler (Hybaid MBS 0.2G Thermal Cycler; Thermo Fisher Scientific, Inc., Waltham, MA, USA). The following primer pairs were used: Oct4-F (5'-GGG ATG GCA TAC TGT GGA C-3'), Oct4-R (5'-CTT CCT CCA CCC ACT TCT C-3'), Sox2-F (5'-GGC GGC AAC CAG AAG AAC AG-3'), Sox2-R (5'-GTT GCT CCA GCC GTT CAT GTG-3'), rat Nanog-F (5'-GCC CTG AGA AGA AAG AAG AG-3'), rat Nanog-R (5'-CGT ACT GCC CCA TAC TGG AA-3') (33), rat nestin-F (5'-AGC CAT TGT GGT CTA CTG A-3'), rat nestin-R (5'-TGC AAC TCT GCC TTA TCC-3'), Sox17-F

(5'-AGG AGA GGT GGT GGC GAG TAG-3'), and Sox17-R (5'-GTT GGG ATG GTC CTG CAT GTG-3') (34).

Western blotting. Cells were harvested and lysed in sodium dodecyl sulfate-polyacrylamide gel electrophoresis (SDS-PAGE) sample buffer (50 mM Tris-HCl, pH 6.8, 2% SDS, and 10% glycerol). Proteins were separated by SDS-PAGE and transferred onto a polyvinylidene fluoride (PVDF) membrane (Millipore). The membrane was blocked with 1% skimmed milk in Tris-buffered saline containing 0.05% Tween-20 and probed with appropriate antibodies using the EnVision System (DakoCytomation, Glostrup, Denmark). Antibody signals were developed using ECL reagents and Hyperfilm ECL film (both from GE Healthcare, Little Chalfont, UK), which were then scanned using CEPROS SV (Fujifilm, Tokyo, Japan). The following primary antibodies were used: anti-Tsc2 antibody (C20; 1:200; Santa Cruz Biotechnology, Inc., Santa Cruz, CA, USA), anti-Tsc1 primary antibody (c-Tsc1, 1:500), anti-phospho-S6 ribosomal protein (Ser235/236) rabbit polyclonal antibody (1:1,000, no. 2211), anti-S6 ribosomal protein rabbit monoclonal antibody (1:1,000, no. 2217) (both from Cell Signaling Technology, Inc., Danvers, MA, USA), and anti-β-actin mouse monoclonal antibody (1:1,000; Sigma-Aldrich).

Embryoid body (EB) formation. ESCs were plated into low-adhesion 96-well dishes (MS-9096; Sumitomo Bakelite Co., Ltd., Tokyo, Japan). After 10 days of suspension culture, EBs were plated onto Matrigel-coated dishes in GMEM/10% fetal bovine serum medium (both from Gibco Life Technologies).

Immunocytochemistry. Cells were fixed and permeabilized with 4% paraformaldehyde and 0.25% Triton X-100 (both from Wako Pure Chemical Industries, Ltd., Osaka, Japan) in PBS for 30 min at 4°C and then washed (3x5 min) with PBS/0.1% bovine serum albumin (BSA) (Iwai Kagaku Co., Tokyo, Japan). Cells were incubated with a primary antibody in PBS with 1% BSA for 1 h at room temperature. Thereafter, cells were washed and incubated with fluorophore-conjugated secondary antibodies and 4',6-diamidino-2-phenylindole (DAPI) for 1 h at room temperature. Immunofluorescent images were captured using a Leica TCS SP5 v2.0 system (Leica, Heidelberg, Germany). The following primary antibodies were used: anti-Oct3/4 mouse monoclonal antibody (1:50, C-10; Santa Cruz Biotechnology, Inc.), anti-Sox2 rabbit polyclonal antibody (1:100, poly6309; BioLegend, San Diego, CA, USA), anti-β-III tubulin mouse monoclonal antibody (1:500, Tuj-1; Covance Laboratories, Princeton, NJ, USA), anti-myosin heavy chain mouse monoclonal antibody (1:50, MF20; R&D Systems, Minneapolis, MN, USA), and anti-Gata4 mouse monoclonal antibody (1:50; Santa Cruz Biotechnology, Inc.). Alexa Fluor (488 or 568)-conjugated goat anti-mouse or goat anti-rabbit secondary antibodies (Invitrogen Life Technologies) were used at 1:1,000 dilutions.

Teratoma formation. Approximately $5x10^5$ cells were injected under kidney capsules of nude mice. Tumors were dissected after 4-5 weeks and fixed in 10% buffered formalin. Tumor tissues were embedded in paraffin wax, sectioned, and examined after hematoxylin and eosin staining.

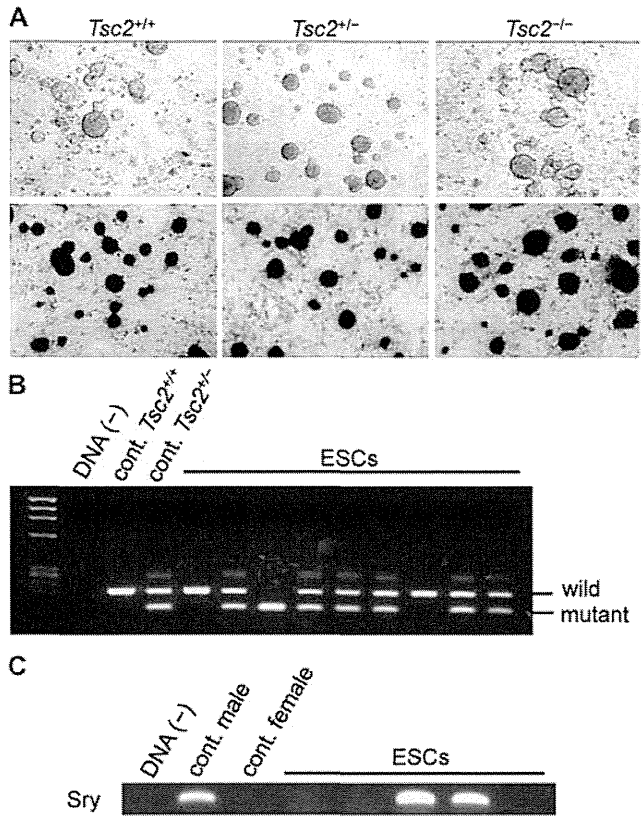

Figure 1. Establishment of *Tsc2*-deficient cell lines from blastocysts of Eker rats. (A) Colonies of established cell lines. $Tsc2^{+/+}$, $Tsc2^{+/-}$, and $Tsc2^{-/-}$ represent wild-type, *Tsc2* heterozygous mutant, and *Tsc2* homozygous mutant, respectively. Morphology of colonies established from blastocysts of Eker rats cultured on mouse embryonic fibroblasts (MEFs) in two inhibitors (2i) with leukemia inhibitory factor (LIF) (upper panels). Alkaline phosphatase staining of colonies (lower panels). Representative colonies are presented. (B) Polymerase chain reaction (PCR) genotyping for the *Tsc2* gene. Upper and lower bands represent wild-type and mutant *Tsc2* alleles, respectively. DNA(-), negative control; cont. $Tsc2^{+/+}$, wild-type rat; cont. $Tsc2^{+/-}$, *Tsc2* heterozygous mutant rat. Results of representative lines [embryonic stem cells (ESCs)] are presented. (C) PCR of the *Sry* gene for gender determination of established cell lines. DNA(-), negative control; cont. male, male control; and cont. female, female control. Results of representative lines (ESCs) are presented.

Blastocyst injection and generation of chimeric rats. Because collection of many blastocysts from Brown Norway rats is inefficient, we attempted the chimera formation assay using Brown Norway as well as Wistar rats. Rat blastocysts at E4.5 days were collected on the day of injection and cultured for 2-3 h to ensure cavitation. ESCs were disaggregated using Accutase, and 10-12 cells were injected into blastocyst cavities. Injected embryos were transferred into uteri of pseudopregnant rats.

Dead embryos were collected from uteri by cesarean section. For *Tsc2* genotyping PCR, genomic DNA was obtained from several parts of each embryo or pup.

Gene expression microarray analysis. The Rat Affymetrix GeneChip Gene 1.0 ST Array (Affymetrix, Inc., Santa Clara, CA, USA) was used for microarray analysis. Amplification and labeling of probes and hybridization were performed according to the manufacturer's instructions. Hierarchical clustering analysis was performed using GeneSpring software version 12.1 (Agilent Technologies, Inc., Santa Clara, CA, USA).

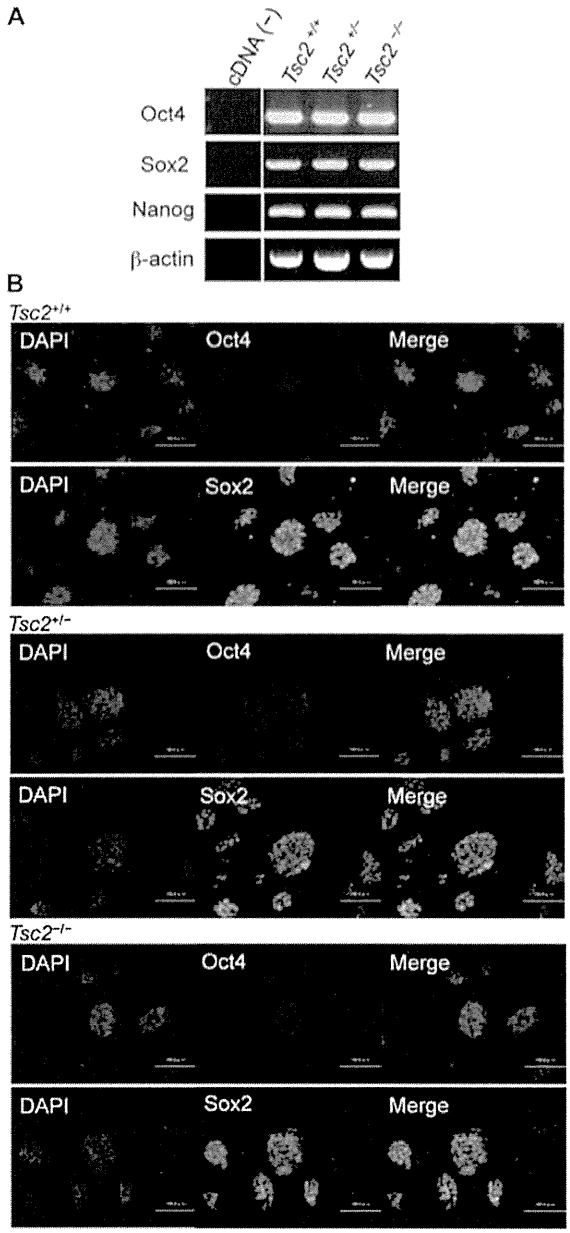

Figure 2. Expression of pluripotency markers in *Tsc2*$^{-/-}$ embryonic stem cells (ESCs). (A) Reverse transcription (RT)-PCR analysis of *Oct4*, *Sox2*, *Nanog*, and *β-actin* expression in established cell lines. cDNA(-); negative control. Representative results are presented. (B) Immunofluorescent staining of pluripotency markers in established cell lines: *Tsc2*$^{+/+}$ (top panels), *Tsc2*$^{+/-}$ (middle panels), and *Tsc2*$^{-/-}$ (bottom panels). Oct4 (red) and Sox2 (green) are used as pluripotency markers. Nuclei are stained with 4',6-diamidino-2-phenylindole (DAPI) (blue). Right panels are merged images of left and center panels. Scale bars, 100 μm.

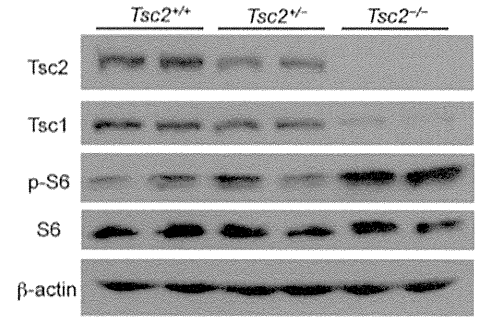

Figure 3. Activated mammalian target of rapamycin complex 1 (mTORC1) pathway in *Tsc2*$^{-/-}$ embryonic stem cells (ESCs). Analysis of mTORC1 pathway activation by western blotting in established cell lines. Tsc1, Tsc2, S6 ribosomal protein (S6), and phosphorylated S6 ribosomal protein (p-S6) were analyzed. β-actin was used as the control.

Results

Establishment of Tsc2-deficient stem cells from Eker rat embryos. After mating of double heterozygous Eker rats, a total of 34 blastocysts were collected. Zonae pellucidae were removed, and most blastocysts were successfully cultured on feeder cells, revealing outgrowths from embryonic fibroblasts (MEFs) in N2B27 medium supplemented with 2i + LIF (33). After several passages, a total of 26 cell lines were established. We routinely passaged these cells every 2-4 days by dissociating them into single cells and replating onto new feeder cells. They grew as dome-shaped or spherical colonies and were maintained for >25 passages without losing their morphology (Fig. 1A). A majority of colonies expressed alkaline phosphatase, an indicator of stem cell character (Fig. 1A). Thereafter, we checked *Tsc2* genotypes of established cell lines by PCR. Surprisingly, we identified that not only *Tsc2*$^{+/+}$ and *Tsc2*$^{+/-}$ cell lines but also *Tsc2*$^{-/-}$ cell lines had been established (Fig. 1B). Considering that previous reports had indicated that *Tsc2* is necessary for the maintenance of stem cell characteristics, this result was unexpected. Both male and female cell lines were established for each genotype (Fig. 1C). Chromosome analysis revealed that most cell lines had normal ploidy (n=42, data not shown). RT-PCR analysis revealed that *Tsc2*$^{-/-}$ cells expressed the pluripotency markers *Oct4*, *Sox2*, and *Nanog* (Fig. 2A). Oct4 and Sox2 expressions were confirmed by immunofluorescence microscopy (Fig. 2B). These results indicate that *Tsc2*-deficient stem cells could be established from Eker rat embryos. We performed further experiments using two independent cell lines of each genotype.

Activation of the mTORC1 pathway in Tsc2$^{-/-}$ *ESCs.* To evaluate the mTORC1 activation status, we analyzed ESCs by western blotting. Tsc2 protein was detected in *Tsc2*$^{+/+}$ and *Tsc2*$^{+/-}$ cells but not in *Tsc2*$^{-/-}$ cells, thereby confirming results of the genotype analysis. Tsc1 protein levels were decreased in *Tsc2*$^{-/-}$ ESCs, thereby reflecting the reciprocal stabilization between Tsc1 and Tsc2 proteins (42). As expected, an increase in S6 phosphorylation was detected in *Tsc2*$^{-/-}$ cells compared with that in *Tsc2*$^{+/+}$ and *Tsc2*$^{+/-}$ cells, which indicates abnormal activation of the mTORC1 pathway in *Tsc2*$^{-/-}$ ESCs (Fig. 3). These results indicate that despite abnormal activation of the mTORC1 pathway, *Tsc2*$^{-/-}$ ESCs can be established.

In vitro differentiation of Tsc2$^{-/-}$ *ESCs into three germ layers.* Using the EB formation assay, we evaluated the differentiation potential of the established cell lines. We assessed the expression of differentiation markers by RT-PCR. Expression of markers for ectoderm (*Nestin*), endoderm (*Sox17*), and mesoderm (*Flk1*) were all observed in EBs (Fig. 4A). We plated EBs onto Matrigel-coated dishes and assessed their differentiation status by immunofluorescent staining for β-III tubulin (neuroectoderm), myosin (mesoderm), and Gata4

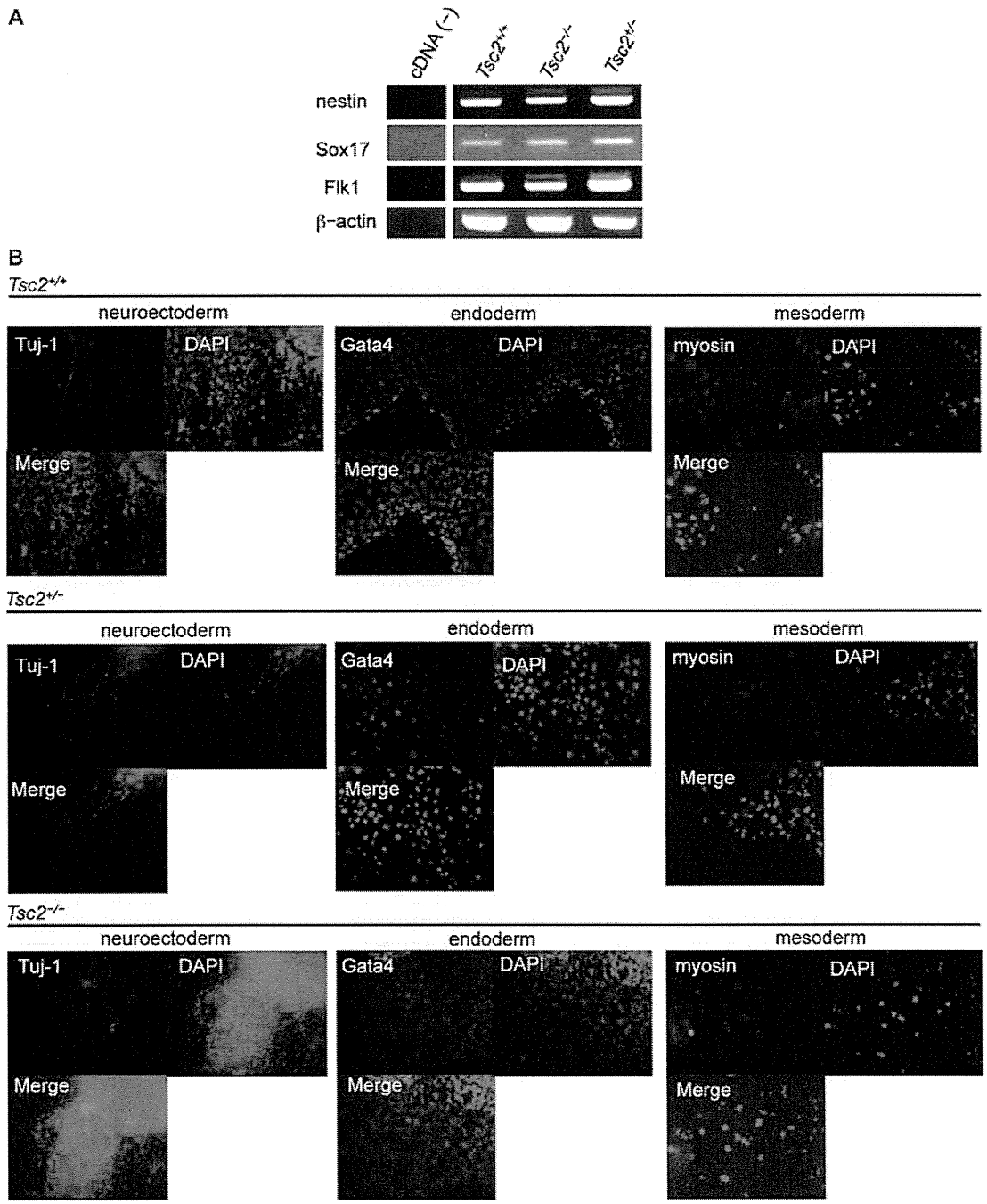

Figure 4. *In vitro* differentiation of *Tsc2*$^{-/-}$ embryonic stem cells (ESCs). (A) Reverse transcription (RT)-PCR analysis of differentiation marker expression in embryoid bodies (EBs) formed from established cell lines. Expression of *Nestin* (ectoderm), *Sox17* (endoderm), and *Flk1* (mesoderm) were analyzed with *β-actin* as control. cDNA(-); negative control. (B) Immunofluorescent staining of Tuj-1/β-III tubulin (neuroectoderm, red), Gata4 (endoderm, red), and myosin (mesoderm, red). Nuclei are stained with 4',6-diamidino-2-phenylindole (DAPI) (blue).

(endoderm) (Fig. 4B). Not only *Tsc2*$^{+/+}$ and *Tsc2*$^{+/-}$ cells but also *Tsc2*$^{-/-}$ cells demonstrated the potential to differentiate into all three germ layers. In addition, we observed spontaneously beating areas in EBs of all *Tsc2* genotypes (data not shown). These results suggest that most differentiation processes of ESCs were not blocked by *Tsc2* deficiency.

Differentiation of Tsc2$^{-/-}$ *ESCs into multiple lineages in teratomas.* When *Tsc2*$^{-/-}$ ESCs were transplanted under the kidney capsule of nude mice, they differentiated into tissues derived from all three germ layers, including gut-like epithelium (endoderm), cartilage and adipocytes (mesoderm), stratified squamous epithelium, and neuroepithelium (ectoderm) (Fig. 5). These results indicate that *Tsc2*$^{-/-}$ ESCs are multipotent, although detailed characterization of each of the differentiated tissues remains to be elucidated. Interestingly, we observed that abnormal ductal structures appeared in *Tsc2*$^{-/-}$ teratomas (Kawano H, *et al,* unpublished data). Further characterization of these abnormal structures is described in another report (Kawano H, *et al,* unpublished data).

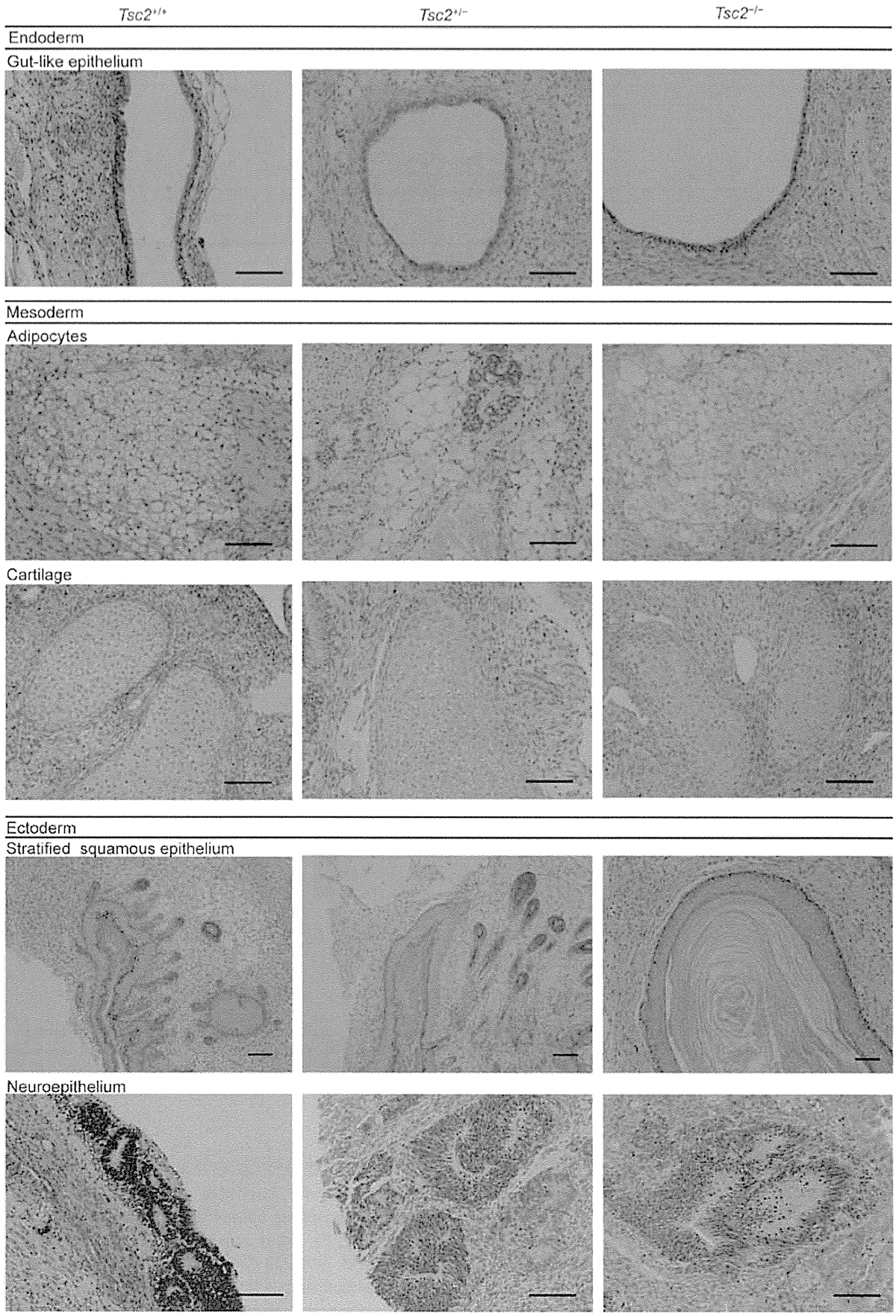

Figure 5. Differentiation of *Tsc2*$^{-/-}$ embryonic stem cells (ESCs) in teratomas. Tissue samples of teratomas derived from established ESCs were stained with hematoxylin and eosin. From top to bottom: gut-like epithelium (endoderm), adipocytes (mesoderm), cartilage (mesoderm), stratified squamous epithelium (ectoderm), and neuroepithelium (ectoderm). Scale bars, 100 μm.

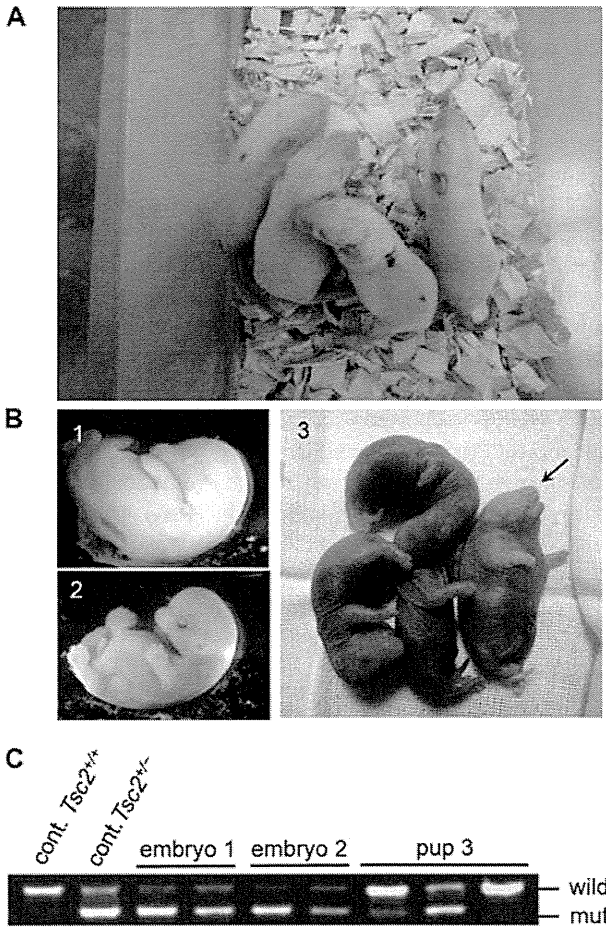

Figure 6. Chimeric rats from established embryonic stem cells (ESCs). (A) Four chimeras (2 males, 2 females) obtained by injection of *Tsc2*$^{+/+}$ ESCs into Wistar blastocysts. Black coat color indicates a contribution of ESCs established from Eker rats. (B) Dead embryos (1 and 2) and a pup (3, arrow) from blastocysts injected with *Tsc2*$^{-/-}$ ESCs. (C) *Tsc2*-genotyping polymerase chain reaction (PCR) of dead embryos and a pup. Genomic DNA was obtained from several parts of each embryo and pup. DNA(-), negative control; cont. *Tsc2*$^{+/+}$, wild-type rat; cont. *Tsc2*$^{+/-}$, *Tsc2* heterozygous mutant rat.

Contribution of Tsc2$^{+/+}$ *ESCs in chimeras.* Next, to determine the ability of established ESCs to form chimeras, we injected *Tsc2*$^{+/+}$ and *Tsc2*$^{-/-}$ ESCs into blastocysts of Wistar rats or Brown Norway rats (Materials and methods). Although ratios were low, four chimeras with black coat color were born from Wistar blastocysts injected with *Tsc2*$^{+/+}$ ESCs, indicating the contribution of ESCs from the Eker rat strain (Fig. 6A). In contrast, we were unable to obtain pups demonstrating chimeric coat color in repeated trials using two independent *Tsc2*$^{-/-}$ ESCs. However, in these trials, we detected dead embryos in the uterus of recipient mother rats at term (Fig. 6B1 and 2). The appearance of dead embryos suggested developmental retardation. In addition, one live pup was delivered by cesarean section but died shortly after birth (Fig. 6B3). This pup revealed various morphological abnormalities such as an enlarged trunk. PCR genotyping of dead embryos and the pup indicated the contribution of *Tsc2*$^{-/-}$ ESCs in their tissues (Fig. 6C). On the basis of the band pattern of two dead embryos, we concluded that they had a greater contribution of *Tsc2*$^{-/-}$ ESCs compared with the live pup. These results suggest that a greater contribution of *Tsc2*$^{-/-}$ ESCs in the chimera results in embryonic lethality.

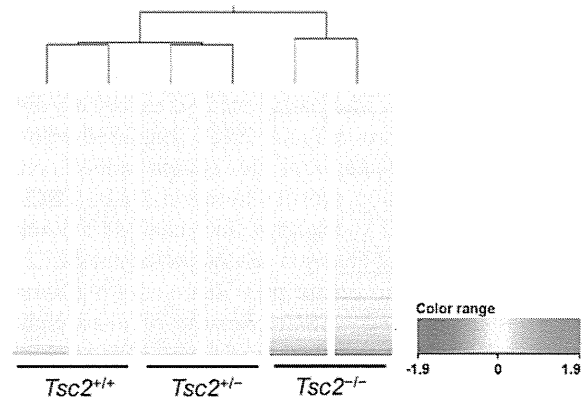

Figure 7. Hierarchical clustering analysis of embryonic stem cells (ESCs). RNAs from ESCs were analyzed using the Affymetrix GeneChip Gene 1.0 ST Array. Data normalization and hierarchical clustering analysis of gene expression profiles were performed using the GeneSpring software.

Although germline transmission has not been confirmed yet, the contribution in chimeras suggests that ESCs established in this study possessed characteristics of multipotent stem cells.

Distinct gene expression pattern in Tsc2$^{-/-}$ *ESCs on microarray analysis.* To compare gene expression profiles of established ESCs, we employed microarray analysis (Fig. 7). Similar expression levels of pluripotency-related genes were identified in all these cells. Moreover, hierarchical clustering analysis revealed that gene expression profiles of *Tsc2*$^{+/+}$ and *Tsc2*$^{+/-}$ ESCs resembled each other, but those of *Tsc2*$^{-/-}$ ESCs revealed an apparently distinct pattern. These results suggest that the homozygous *Tsc2* mutation causes extensive gene expression changes in rat ESCs.

Discussion

In this study, we successfully established *Tsc2*$^{-/-}$ ESCs from Eker rats. These cells possessed characteristic features of ESCs, including expression of pluripotency markers, long-term self-renewal, and the capacity to differentiate into derivatives of all three germ layers. Although detailed mechanisms are still not clear, there have been several reports indicating the importance of the Tsc2-mTOR pathway in stem cell maintenance and differentiation (38,39,43). Gan *et al* reported that *Tsc1* is a critical regulator of self-renewal, mobilization, and multilineage development in hematopoietic stem cells and that it executes these phenomena via both mTORC1-dependent and -independent pathways (39). Further, it was reported that the activation of S6K by expression of the constitutively active S6K1 or siRNA-mediated knockdown of *TSC2* and *RICTOR* induced differentiation of human ESCs (38). Recently, Betschinger *et al* reported that siRNA-mediated knockdown of *Tsc2* or *Flcn* inhibits differentiation of ESCs (43). In contrast to results in these reports, we successfully established *Tsc2*$^{-/-}$ ESCs possessing multipotent differentiation capacity despite the presence of the activated mTORC1 pathway. There are several possible reasons why the derivation of *Tsc2*$^{-/-}$ ESCs was possible in this study. Previous studies utilized siRNA- or shRNA-mediated knockdown of *Tsc2* in already established ESCs or conditional knockout of *Tsc1* in

somatic stem cells. Such 'acute' downregulation of *Tsc1/Tsc2* may cause some aberrant gene regulation that restrains the maintenance of the multipotent nature and differentiation capacity of stem cells. Microarray analysis revealed a distinct gene expression pattern in $Tsc2^{-/-}$ ESCs compared with their $Tsc2^{+/+}$ and $Tsc2^{+/-}$ counterparts. Our system enables comparison of gene expression profiles between $Tsc2^{-/-}$ ESCs and $Tsc2^{+/-}$ ESCs with *Tsc2* knockdown. Such analysis is of interest to further explore *Tsc2* mutation-related pathogenesis.

We were unable to obtain pups demonstrating chimeric coat color using $Tsc2^{-/-}$ ESCs. Results of dead embryos suggested that higher contribution of $Tsc2^{-/-}$ cells in chimeras induced embryonic lethality. Further, it has been reported that when human *TSC2*-deficient fibroblast-like cells were grafted into mice, differentiated tissues revealed features of TSC skin tumors and that *TSC2*-deficient cells directly or indirectly induce abnormal follicular neogenesis and epidermal proliferation (44). Because $Tsc2^{-/-}$ ESCs may cause abnormal differentiation of hair in chimeras, it may not be appropriate to determine the contribution of ESCs on the basis of hair color of chimeras.

He *et al* reported that reprogramming of somatic cells derived from $Tsc2^{-/-}$ mouse embryos to iPSCs was not possible (40). In this study, we provide evidence that the derivation of $Tsc2^{-/-}$ ESCs from Eker rat embryos is possible. In somatic cells, some epigenetic abnormalities caused by *Tsc2* deficiency may not be corrected even under reprogramming conditions. Conversely, during early embryogenesis, epigenetic abnormalities in $Tsc2^{-/-}$ cells may be tuned to maintain the stemness. With reprogramming experiments using Eker rat-derived embryonic fibroblasts, ESCs established in this study will serve as useful tools to compare effects of *Tsc2* deficiency on epigenetic status in reprogramming and ESC derivation.

In recent years, various patient-derived iPSCs have been used for *in vitro* differentiation experiments to mimic the pathogenesis of human diseases (45,46). Moreover, such cellular models are useful to research novel drug target molecules by high-throughput screening (47). With regard to tumorigenesis, tissue specificity and abnormal differentiation are relevant to its molecular basis. Lineage-specific *in vitro* differentiation of tumor suppressor-deficient ESCs will provide valuable experimental models to explore the mechanism of pathogenesis. However, in humans, establishment of tumor suppressor-deficient (i.e., homozygously inactivated) ESCs or iPSCs has been technically difficult. In rodents, homozygous mutant ESCs for tumor suppressors, including *Rb*, *Tp53*, and *Apc*, have been established (48-50). To date, none of those ESCs have been extensively used for *in vitro* differentiation experiments. For example, *Apc*-deficient ESCs failed to differentiate into multiple lineages in the teratoma formation assay, suggesting that the induction of various cell types was not applicable to these ESCs (50). In contrast, $Tsc2^{-/-}$ ESCs exhibited the potential to differentiate into all germ layers and multiple cell lineages, both *in vitro* and *in vivo*. We already observed development of abnormal ductal structures in $Tsc2^{-/-}$ teratomas, suggesting that cell type-specific effects of *Tsc2* deficiency could be reproduced in differentiation of ESCs (Kawano H, *et al*, unpublished data). Combined with *in vivo* experiments, *in vitro* differentiation models using ESCs established in this study will facilitate understanding of *Tsc2* mutation-related pathogenesis as well as aid in the search for therapeutic target pathways.

Acknowledgements

We thank Takako Ikegami, and Tomomi Ikeda, Laboratory of Molecular and Biochemical Research, Research Support Center, Juntendo University Graduate School of Medicine (Tokyo, Japan) for technical assistance. The authors would like to thank Enago (www.enago.jp) for the English language review. This study was supported in part by the following grants: Grants-in-Aid for Scientific Research from the Ministry of Education, Culture, Sports, Science and Technology (MEXT) (Japan); MEXT-Supported Program for the Strategic Research Foundation at Private Universities; Grants-in-Aid for Scientific Research from the Japan Society for the Promotion of Science (Japan); and Grants-in-Aid for Scientific Research from the Ministry of Health, Labour and Welfare (Japan). This study was also supported by the Research Institute for Diseases of Old Age, Juntendo University Graduate School of Medicine.

References

1. Kwiatkowski DJ, Whittemore VH and Thiele EA (eds): Tuberous Sclerosis Complex: Genes, Clinical Features, and Therapeutics. Wiley-VCH Verlag GmbH & Co. KGaA, Weinheim, 2010.
2. European Chromosome 16 Tuberous Sclerosis Consortium: Identification and characterization of the tuberous sclerosis gene on chromosome 16. Cell 75: 1305-1315, 1993.
3. van Slegtenhorst M, de Hoogt R, Hermans C, *et al*: Identification of the tuberous sclerosis gene TSC1 on chromosome 9q34. Science 277: 805-808, 1997.
4. Curatolo P, Bombardieri R and Jozwiak S: Tuberous sclerosis. Lancet 372: 657-668, 2008.
5. Laplante M and Sabatini DM: mTOR signaling in growth control and disease. Cell 149: 274-293, 2012.
6. Knudson AG Jr: Mutation and cancer: Statistical study of retinoblastoma. Proc Natl Acad Sci USA 68: 820-823, 1971.
7. Henske EP, Scheithauer BW, Short MP, Wollmann R, Nahmias J, Hornigold N, van Slegtenhorst M, Welsh CT and Kwiatkowski DJ: Allelic loss is frequent in tuberous sclerosis kidney lesions but rare in brain lesions. Am J Hum Genet 59: 400-406, 1996.
8. Au KS, Hebert AA, Roach ES and Northrup H: Complete inactivation of the TSC2 gene leads to formation of hamartomas. Am J Hum Genet 65: 1790-1795, 1999.
9. Tucker T and Friedman JM: Pathogenesis of hereditary tumors: Beyond the 'two-hit' hypothesis. Clin Genet 62: 345-357, 2002.
10. Chan JA, Zhang H, Roberts PS, Jozwiak S, Wieslawa G, Lewin-Kowalik J, Kotulska K and Kwiatkowski DJ: Pathogenesis of tuberous sclerosis subependymal giant cell astrocytomas: Biallelic inactivation of TSC1 or TSC2 leads to mTOR activation. J Neuropathol Exp Neurol 63: 1236-1242, 2004.
11. Niida Y, Stemmer-Rachamimov AO, Logrip M, Tapon D, Perez R, Kwiatkowski DJ, Sims K, MacCollin M, Louis DN and Ramesh V: Survey of somatic mutations in tuberous sclerosis complex (TSC) hamartomas suggests different genetic mechanisms for pathogenesis of TSC lesions. Am J Hum Genet 69: 493-503, 2001.
12. Onda H, Lueck A, Marks PW, Warren HB and Kwiatkowski DJ: Tsc2(+/-) mice develop tumors in multiple sites that express gelsolin and are influenced by genetic background. J Clin Invest 104: 687-695, 1999.
13. Kobayashi T, Minowa O, Kuno J, Mitani H, Hino O and Noda T: Renal carcinogenesis, hepatic hemangiomatosis, and embryonic lethality caused by a germ-line Tsc2 mutation in mice. Cancer Res 59: 1206-1211, 1999.
14. Kobayashi T, Minowa O, Sugitani Y, Takai S, Mitani H, Kobayashi E, Noda T and Hino O: A germ-line Tsc1 mutation causes tumor development and embryonic lethality that are similar, but not identical to, those caused by Tsc2 mutation in mice. Proc Natl Acad Sci USA 98: 8762-8767, 2001.

15. Meikle L, Pollizzi K, Egnor A, Kramvis I, Lane H, Sahin M and Kwiatkowski DJ: Response of a neuronal model of tuberous sclerosis to mammalian target of rapamycin (mTOR) inhibitors: Effects on mTORC1 and Akt signaling lead to improved survival and function. J Neurosci 28: 5422-5432, 2008.
16. Goorden SMI, van Woerden GM, van der Weerd L, Cheadle JP and Elgersma Y: Cognitive deficits in $Tsc1^{+/-}$ mice in the absence of cerebral lesions and seizures. Ann Neurol 62: 648-655, 2007.
17. Ehninger D, Han S, Shilyansky C, Zhou Y, Li W, Kwiatkowski DJ, Ramesh V and Silva AJ: Reversal of learning deficits in a $Tsc2^{+/-}$ mouse model of tuberous sclerosis. Nat Med 14: 843-848, 2008.
18. Eker R and Mossige J: A dominant gene for renal adenomas in the rat. Nature 189: 858-859, 1961.
19. Hino O, Mitani H and Knudson AG: Genetic predisposition to transplacentally induced renal cell carcinomas in the Eker rat. Cancer Res 53: 5856-5858, 1993.
20. Kobayashi T, Hirayama Y, Kobayashi E, Kubo Y and Hino O: A germline insertion in the tuberous sclerosis (Tsc2) gene gives rise to the Eker rat model of dominantly inherited cancer. Nat Genet 9: 70-74, 1995.
21. Rennebeck G, Kleymenova EV, Anderson R, Yeung RS, Artzt K and Walker CL: Loss of function of the tuberous sclerosis 2 tumor suppressor gene results in embryonic lethality characterized by disrupted neuroepithelial growth and development. Proc Natl Acad Sci USA 95: 15629-15634, 1998.
22. Mizuguchi M, Takashima S, Yamanouchi H, Nakazato Y, Mitani H and Hino O: Novel cerebral lesions in the Eker rat model of tuberous sclerosis: Cortical tuber and anaplastic ganglioglioma. J Neuropathol Exp Neurol 59: 188-196, 2000.
23. Yeung RS, Katsetos CD and Klein-Szanto A: Subependymal astrocytic hamartomas in the Eker rat model of tuberous sclerosis. Am J Pathol 151: 1477-1486, 1997.
24. Takahashi DK, Dinday MT, Barbaro NM and Baraban SC: Abnormal cortical cells and astrocytomas in the Eker rat model of tuberous sclerosis complex. Epilepsia 45: 1525-1530, 2004.
25. Prabhakar S, Goto J, Zhang X, *et al*: Stochastic model of Tsc1 lesions in mouse brain. PLoS One 8: e64224, 2013.
26. Kobayashi T, Adachi H, Mitani H, Hirayama Y and Hino O: Toward chemotherapy for Tsc2-mutant renal tumor. Proc Jpn Acad 79: 22-25, 2003.
27. Kenerson HL, Aicher LD, True LD and Yeung RS: Activated mammalian target of rapamycin pathway in the pathogenesis of tuberous sclerosis complex renal tumors. Cancer Res 62: 5645-5650, 2002.
28. Lee L, Sudentas P, Donohue B, *et al*: Efficacy of a rapamycin analog (CCI-779) and IFN-γ in tuberous sclerosis mouse models. Genes Chromosomes Cancer 42: 213-227, 2005.
29. McCormack FX, Inoue Y, Moss J, *et al*; National Institutes of Health Rare Lung Diseases Consortium; MILES Trial Group: Efficacy and safety of sirolimus in lymphangioleiomyomatosis. N Engl J Med 364: 1595-1606, 2011.
30. Franz DN, Belousova E, Sparagana S, *et al*: Efficacy and safety of everolimus for subependymal giant cell astrocytomas associated with tuberous sclerosis complex (EXIST-1): A multicentre, randomised, placebo-controlled phase 3 trial. Lancet 381: 125-132, 2013.
31. Bissler JJ, Kingswood JC, Radzikowska E, *et al*: Everolimus for angiomyolipoma associated with tuberous sclerosis complex or sporadic lymphangioleiomyomatosis (EXIST-2): A multicentre, randomised, double-blind, placebo-controlled trial. Lancet 381: 817-824, 2013.
32. Mizuguchi M: Abnormal giant cells in the cerebral lesions of tuberous sclerosis complex. Congenit Anom (Kyoto) 47: 2-8, 2007.
33. Buehr M, Meek S, Blair K, Yang J, Ure J, Silva J, McLay R, Hall J, Ying QL and Smith A: Capture of authentic embryonic stem cells from rat blastocysts. Cell 135: 1287-1298, 2008.
34. Li P, Tong C, Mehrian-Shai R, *et al*: Germline competent embryonic stem cells derived from rat blastocysts. Cell 135: 1299-1310, 2008.
35. Evans MJ and Kaufman MH: Establishment in culture of pluripotential cells from mouse embryos. Nature 292: 154-156, 1981.
36. Martin GR: Isolation of a pluripotent cell line from early mouse embryos cultured in medium conditioned by teratocarcinoma stem cells. Proc Natl Acad Sci USA 78: 7634-7638, 1981.
37. Thomson JA, Itskovitz-Eldor J, Shapiro SS, Waknitz MA, Swiergiel JJ, Marshall VS and Jones JM: Embryonic stem cell lines derived from human blastocysts. Science 282: 1145-1147, 1998.
38. Easley CA IV, Ben-Yehudah A, Redinger CJ, Oliver SL, Varum ST, Eisinger VM, Carlisle DL, Donovan PJ and Schatten GP: mTOR-mediated activation of p70 S6K induces differentiation of pluripotent human embryonic stem cells. Cell Reprogram 12: 263-273, 2010.
39. Gan B, Sahin E, Jiang S, Sanchez-Aguilera A, Scott KL, Chin L, Williams DA, Kwiatkowski DJ and DePinho RA: mTORC1-dependent and -independent regulation of stem cell renewal, differentiation, and mobilization. Proc Natl Acad Sci USA 105: 19384-19389, 2008.
40. He J, Kang L, Wu T, *et al*: An elaborate regulation of Mammalian target of rapamycin activity is required for somatic cell reprogramming induced by defined transcription factors. Stem Cells Dev 21: 2630-2641, 2012.
41. Shiono M, Kobayashi T, Takahashi R, *et al*: The G1556S-type tuberin variant suppresses tumor formation in tuberous sclerosis 2 mutant (Eker) rats despite its deficiency in mTOR inhibition. Oncogene 27: 6690-6697, 2008.
42. Benvenuto G, Li S, Brown SJ, Braverman R, Vass WC, Cheadle JP, Halley DJ, Sampson JR, Wienecke R and DeClue JE: The tuberous sclerosis-1 (TSC1) gene product hamartin suppresses cell growth and augments the expression of the TSC2 product tuberin by inhibiting its ubiquitination. Oncogene 19: 6306-6316, 2000.
43. Betschinger J, Nichols J, Dietmann S, Corrin PD, Paddison PJ and Smith A: Exit from pluripotency is gated by intracellular redistribution of the bHLH transcription factor Tfe3. Cell 153: 335-347, 2013.
44. Li S, Thangapazham RL, Wang JA, Rajesh S, Kao TC, Sperling L, Moss J and Darling TN: Human TSC2-null fibroblast-like cells induce hair follicle neogenesis and hamartoma morphogenesis. Nat Commun 2: 235, 2011.
45. Ebert AD, Yu J, Rose FF Jr, Mattis VB, Lorson CL, Thomson JA and Svendsen CN: Induced pluripotent stem cells from a spinal muscular atrophy patient. Nature 457: 277-280, 2009.
46. Lee G, Papapetrou EP, Kim H, *et al*: Modelling pathogenesis and treatment of familial dysautonomia using patient-specific iPSCs. Nature 461: 402-406, 2009.
47. Yang YM, Gupta SK, Kim KJ, *et al*: A small molecule screen in stem-cell-derived motor neurons identifies a kinase inhibitor as a candidate therapeutic for ALS. Cell Stem Cell 12: 713-726, 2013.
48. Williams BO, Schmitt EM, Remington L, Bronson RT, Albert DM, Weinberg RA and Jacks T: Extensive contribution of Rb-deficient cells to adult chimeric mice with limited histopathological consequences. EMBO J 13: 4251-4259, 1994.
49. Kawamata M and Ochiya T: Two distinct knockout approaches highlight a critical role for p53 in rat development. Sci Rep 2: 945, 2012.
50. Kielman MF, Rindapää M, Gaspar C, van Poppel N, Breukel C, van Leeuwen S, Taketo MM, Roberts S, Smits R and Fodde R: Apc modulates embryonic stem-cell differentiation by controlling the dosage of beta-catenin signaling. Nat Genet 32: 594-605, 2002.

Published online: February 19, 2015

Scientific Report

TRANSPARENT PROCESS

EMBO reports

Distinct germline progenitor subsets defined through Tsc2–mTORC1 signaling

Robin M Hobbs[1,2,**], Hue M La[2], Juho-Antti Mäkelä[2], Toshiyuki Kobayashi[3], Tetsuo Noda[4] & Pier Paolo Pandolfi[1,*]

Abstract

Adult tissue maintenance is often dependent on resident stem cells; however, the phenotypic and functional heterogeneity existing within this self-renewing population is poorly understood. Here, we define distinct subsets of undifferentiated spermatogonia (spermatogonial progenitor cells; SPCs) by differential response to hyperactivation of mTORC1, a key growth-promoting pathway. We find that conditional deletion of the mTORC1 inhibitor *Tsc2* throughout the SPC pool using *Vasa-Cre* promotes differentiation at the expense of self-renewal and leads to germline degeneration. Surprisingly, *Tsc2* ablation within a subset of SPCs using *Stra8-Cre* did not compromise SPC function. SPC activity also appeared unaffected by *Amh-Cre*-mediated *Tsc2* deletion within somatic cells of the niche. Importantly, we find that differentiation-prone SPCs have elevated mTORC1 activity when compared to SPCs with high self-renewal potential. Moreover, SPCs insensitive to *Tsc2* deletion are preferentially associated with mTORC1-active committed progenitor fractions. We therefore delineate SPC subsets based on differential mTORC1 activity and correlated sensitivity to *Tsc2* deletion. We propose that mTORC1 is a key regulator of SPC fate and defines phenotypically distinct SPC subpopulations with varying propensities for self-renewal and differentiation.

Keywords differentiation; germline stem cells; mTORC1
Subject Category Stem Cells
DOI 10.15252/embr.201439379 | Received 31 July 2014 | Revised 17 December 2014 | Accepted 15 January 2015

Introduction

It is becoming apparent that the stem cell populations of tissues are heterogeneous in nature [1]. Discrete subpopulations of stem cells have been identified within the same cell lineage that possess the defining stem cell property of self-renewal but differ in their lifespan, cell cycle status and contribution to tissue regeneration [2,3]. The existence of functionally distinct stem cell subtypes within the same tissue is suggested to underlie effective homeostasis and regeneration following injury [4]. The hierarchical relationship between these stem cell subsets is of great interest, as are the molecular mechanisms responsible for defining their divergent functional properties. Key to identification of stem cell subpopulations is the availability of transgenic reporter strains showing restricted expression within the phenotypically distinct stem cell subsets that allows cellular fate mapping [1,2].

Continual production of spermatozoa in the mouse testis is dependent on a resident population of undifferentiated spermatogonia with self-renewal potential (referred to here as spermatogonial stem/progenitor cells; SPCs) [5,6]. The SPC pool of adult mice is composed of isolated single cells (A-single spermatogonia or A_s) and cysts of cells that remain interconnected by cytoplasmic bridges after cell division; 2-cell cysts are referred to as A-paired (A_{pr}) spermatogonia while chains of four or more cells as A-aligned (A_{al}). SPC differentiation is marked by induction of the receptor tyrosine kinase c-Kit and a series of rapid mitotic divisions prior to meiosis. While most cells within the SPC pool are proposed to have stem cell potential, heterogeneity at the levels of cellular morphology and gene expression predicts differing propensities for self-renewal and differentiation. SPCs expressing *Neurogenin 3* (*Ngn3*), typically A_{al}, are predisposed to differentiate [7]. Conversely, SPCs expressing *Gfra1*, a component of the glial cell line-derived neurotrophic factor (GDNF) receptor, predominantly A_s and A_{pr}, are more likely to act as stem cells [7,8]. In the steady-state, self-renewal is largely restricted to $Gfr\alpha1^+$ cells, which then generate $Ngn3^+$ cysts that in turn generate c-Kit^+ differentiating spermatogonia. However, $Ngn3^+$ A_{al} cells can fragment to shorter cysts or A_s cells and revert these characteristic gene expression patterns [7]. Thus, although a large fraction of the SPC pool is primed to differentiate, the cells retain the capacity to generate a long-lived stem cell population, a potential that is most evident upon transplantation or during testis regeneration [7,9]. However, the mechanisms that dictate the varying self-renewal and differentiation propensities of SPC subsets remain poorly understood.

1 Cancer Research Institute, Beth Israel Deaconess Cancer Center, Department of Medicine and Pathology, Beth Israel Deaconess Medical Center, Harvard Medical School, Boston, MA, USA
2 Australian Regenerative Medicine Institute and Department of Anatomy and Developmental Biology, Monash University, Clayton, VIC, Australia
3 Department of Pathology and Oncology, Juntendo University School of Medicine, Tokyo, Japan
4 Department of Cell Biology, JFCR Cancer Institute, Tokyo, Japan
*Corresponding author. Tel: +1 617 735 2145; Fax: +1 617 735 2120; E-mail: ppandolf@bidmc.harvard.edu
**Corresponding author. Tel: +61 3 9902 9611; Fax: +61 3 9902 9729; E-mail: robin.hobbs@monash.edu

The *promyelocytic leukemia zinc finger* (*Plzf*) gene, encoding a POZ-*Krüppel* (POK) family transcription factor, is essential for germline maintenance of the mouse and SPC self-renewal *in vivo* [10,11]. Importantly, Plzf is expressed by all cells within the SPC pool and is a well-established marker of this cell population [6,12]. Through study of the $Plzf^{-/-}$ mouse, we have previously implicated the mTORC1 signaling pathway as a critical regulator of SPC fate decisions [6]. Specifically, SPCs lacking *Plzf* display an aberrant tendency to differentiate rather than self-renew, an effect at least partially dependent on the ability of Plzf to inhibit mTORC1 through transcriptional modulation of the upstream regulator *Redd1*. This study highlights a common feature of tissue-specific stem cell compartments, the detrimental effects of aberrant mTORC1 activation on self-renewal [13–16].

The mTORC1 signaling complex is a central positive regulator of cell growth and is regulated by diverse stimuli including growth factor signaling, nutrient availability and cellular stress in order to balance anabolic and catabolic processes appropriate to the cellular environment [17]. While the mTORC1 pathway induces protein synthesis by stimulating cap-dependent mRNA translation, it can also regulate discrete gene expression programs at both transcriptional and translational levels [18–20]. In addition, mTORC1 activation drives specific bio-energetic and metabolic pathways in order to support increased cell growth [17]. Critically, mTORC1 has emerged as a key regulator of stem cell function plus aging and is commonly involved in the development of cancer.

In order to fully assess the role played by mTORC1 in control of SPC fate, and whether cell-autonomous and non-cell-autonomous contributions could be relevant to its role in SPC fate determination, we have developed mouse models with conditional deletion of *Tsc2*, a critical upstream inhibitor of mTORC1, within distinct cell populations of the testis. In combination with a detailed assessment of mTORC1 activity within the progenitor pool, our data conclusively define the functional role played by mTORC1 in control of SPC heterogeneity and differentiation commitment.

Results and Discussion

Distinct cell types of testis exhibit mTORC1 activation

As the role played by the mTORC1 signaling pathway in male germline regulation remains poorly defined, we first analyzed adult wild-type testis for evidence of mTORC1 activation. To this end, we used phosphorylation of ribosomal protein S6 (RPS6) as an indirect readout of mTORC1 activity [6,17]. Immunohistochemistry (IHC) for P-RPS6 revealed that both germ cells and somatic cells within the testis activate mTORC1 in the steady-state adult tissue (Fig 1A). P-RPS6 was present in a characteristic cytoplasmic staining pattern and more evident at certain stages of the cycling seminiferous epithelium than others [21] (Fig 1A and unpublished observations). P-RPS6-positive cells that were present on the basement membrane of the seminiferous tubules and identified as spermatogonia by morphology were most apparent in stage II–VI tubules when populations of differentiating spermatogonia are abundant. Further, P-RPS6 was detected in the cytoplasm of Sertoli cells, the critical somatic supportive cell of spermatogenesis, extending from the basement membrane toward the tubule lumen. P-RPS6-positive Sertoli cells were concentrated in late-stage VIII tubules, where one generation of mature spermatids has just been released into the tubule lumen and differentiating spermatogonia undergo their first mitotic division. These data suggest that coordinated mTORC1 activation can play a role in spermatogenesis.

In order to determine whether the SPC pool within testis showed evidence of mTORC1 activation, we performed whole-mount immunostaining of adult seminiferous tubules for P-RPS6 and Plzf, an established marker of SPCs [6,10,11]. Importantly, P-RPS6 was mostly detected in differentiating spermatogonia, characterized by low Plzf expression and long cyst length (Fig 1B). These data suggested that mTORC1 activation was limited within the undifferentiated spermatogonial pool, consistent with the ability of Plzf to negatively regulate this pathway [6]. However, mTORC1-dependent RPS6 phosphorylation is indirect and dependent on the activation of downstream RPS6 kinases (S6K1 and 2) that integrate additional regulatory inputs besides mTORC1 [22]. Moreover, S6K is a relatively poor substrate for the mTORC1 kinase complex when compared to other direct targets such as eukaryotic translation initiation factor 4E binding protein 1 (4EBP1), a key downstream regulator of mRNA translation [22,23]. Therefore, we next assessed 4EBP1 phosphorylation as a more sensitive and direct measure of mTORC1 activity within the SPC pool. Whole-mount analysis of adult seminiferous tubules revealed a striking heterogeneous staining for phospho-4EBP1 within the Plzf-positive SPC population (Fig 1C). Phospho-4EBP1 was also detected in populations of differentiating spermatogonia (unpublished observations). Importantly, we observed a significant and positive correlation between 4EBP1 phosphorylation and increasing SPC cyst lengths (Fig 1C and D). While a limited fraction of shorter cysts (A_s and A_{pr}) were phospho-4EBP1 positive (25–36% respectively), longer A_{al} cysts were frequently labeled and approximately 90% of A_{al} cysts containing 8 or more cells were phospho-4EBP1 positive. Conversely, an antibody specific for non-phosphorylated 4EBP1 labeled Plzf-positive A_s and A_{pr} cells while longer A_{al} cysts were generally negative (Fig 1E). Interestingly, we noted that germ cells at later differentiation stages (B spermatogonia/pre-leptotene cells) were also positive for non-phosphorylated 4EBP1, indicating dynamic regulation of this pathway during spermatogenesis (Fig 1E). Given that increasing SPC cyst length is associated with an enhanced tendency to differentiate [7], our results suggested that mTORC1 activity was correlated with differentiation commitment within the progenitor pool. In an effort to confirm this observation, we assessed the phosphorylation status of 4EBP1 within the Gfrα1-positive fraction of SPCs containing the majority of self-renewing cells under steady-state conditions [7,8]. Noticeably, Gfrα1-positive cells (typically A_s and A_{pr}) were rarely positive for phospho-4EBP1, with only approximately 15% labeled (Fig 1F; Supplementary Fig S1A and B). In contrast, expression of Lin28a, suggested to preferentially mark differentiation-committed cells within the SPC pool, was strongly associated with 4EBP1 phosphorylation levels (Supplementary Fig S1C) [24]. Together, these data demonstrate that mTORC1 activity is suppressed in the self-renewing population but induced in committed progenitors, indicating a potential role for this pathway in SPC fate decisions.

Hyperactivation of mTORC1 by germ cell-specific deletion of Tsc2

In order to dissect a potential cell-autonomous role for mTORC1 in SPC function, we next sought to genetically perturb mTORC1

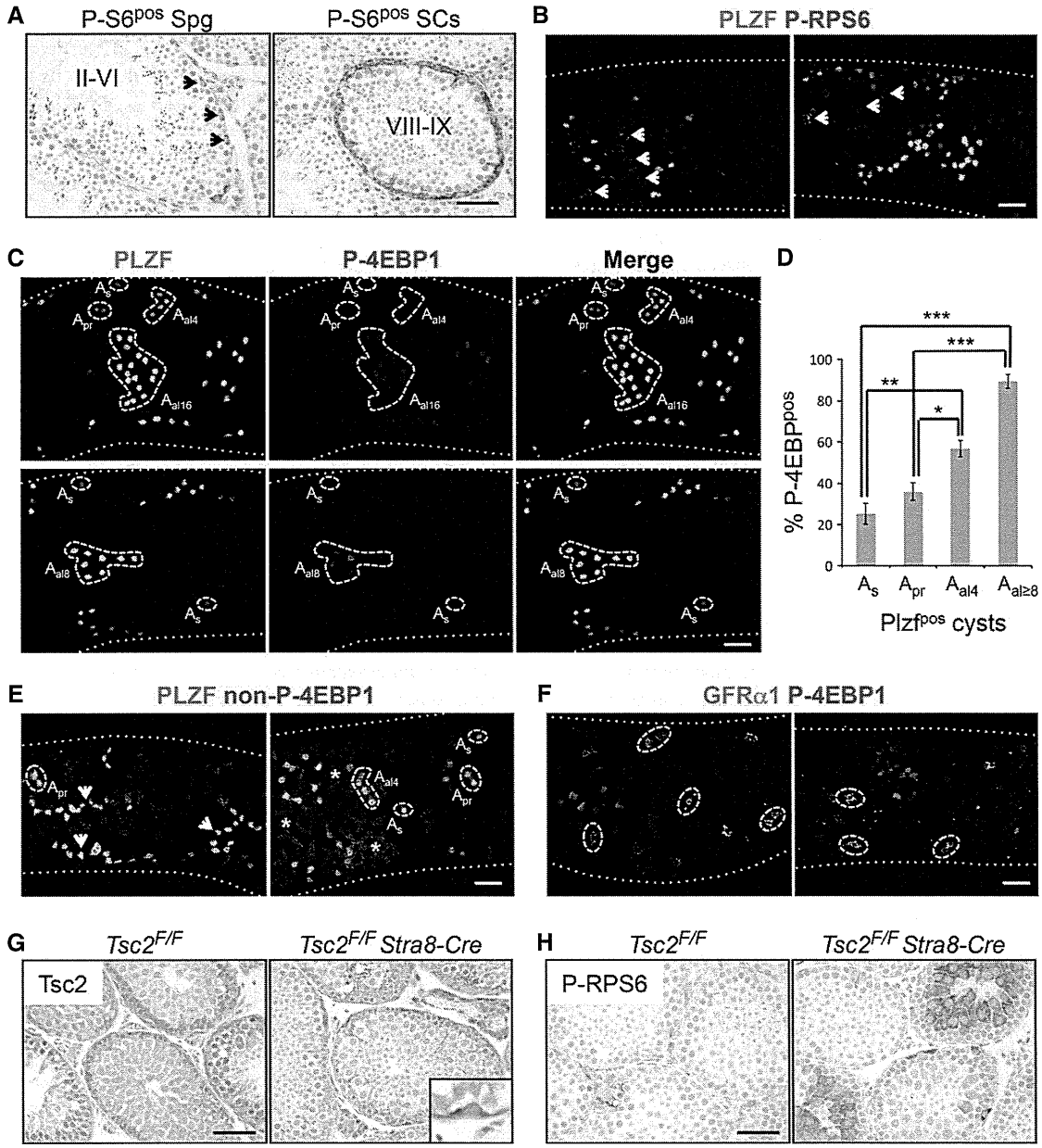

Figure 1. Analysis of mTORC1 pathway activation in testis germ cells.

A Immunohistochemistry (IHC) of adult wild-type testis for P-RPS6. Left and right panels show P-RPS6-positive spermatogonia (Spg, indicated by arrowheads) and Sertoli cells (SCs), respectively. Seminiferous tubules stages are shown.

B Representative whole-mount images of wild-type adult seminiferous tubules stained for PLZF and phospho-RPS6. Arrowheads indicate P-RPS6-positive differentiating spermatogonia with low or absent Plzf expression. Duplicate animals were analyzed.

C Representative whole-mount images of wild-type adult seminiferous tubules stained for PLZF and phospho-4EBP1. Dashed outlines indicate Plzf-positive cysts of varying lengths.

D Quantification of whole-mount analysis from (C). Graph displays percentage of Plzf-positive cysts of indicated lengths that are positive for P-4EBP1. Mean values from three independent animals are shown ± SEM. More than 450 cysts were scored per sample and significant differences are indicated. *$P < 0.05$; **$P < 0.01$; ***$P < 0.001$.

E Representative whole-mount images of wild-type adult seminiferous tubules stained for PLZF and non-phospho-4EBP1. Dashed outlines indicate short Plzf-positive cysts containing non-phospho-4EBP1. Arrowheads indicate longer A_{al} chains negative for non-phospho-4EBP1. Asterisks mark non-phospho-4EBP1-positive differentiating B spermatogonia/pre-leptotene cells.

F Representative whole-mount images of wild-type adult seminiferous tubules stained for Gfrα1 and phospho-4EBP1. Dashed outlines indicate Gfrα1-positive cysts.

G Representative IHC for Tsc2 on sections of testis from 3 weeks postnatal mice of the indicated genotypes. Higher magnification inset shows an example spermatogonium retaining Tsc2 expression.

H Representative IHC for P-RPS6 on testis sections as in (G).

Data information: Scale bars are 50 μm. Dotted lines in whole mounts indicate the seminiferous tubule profile.

activity in a germ cell-specific fashion. To this end, we developed a conditional knockout mouse model for *Tuberous sclerosis 2* (*Tsc2*), which encodes a key negative regulator of the mTORC1 pathway. Tsc2 functions in a heterodimeric complex with the unrelated protein Tsc1 and possesses GTPase-activating protein (GAP) activity toward the small G-protein Rheb, a potent activator of mTORC1 when in a GTP-bound state. As whole-body knockout of either *Tsc1* or *Tsc2* results in embryonic lethality [25,26], we at first crossed mice carrying floxed alleles of *Tsc2* with transgenic mice expressing *Cre* recombinase from proximal elements of the *Stra8* promoter [27]. *Stra8-Cre* drives efficient floxed (F) gene deletion in the postnatal male germline and is active in a substantial fraction of the Plzf-expressing SPC pool plus differentiating spermatogonia and pre-meiotic cells [12,27].

Strikingly, analysis of juvenile (3 weeks postnatal) $Tsc2^{F/F}$ *Stra8-Cre* testis revealed no obvious phenotype; thus, we performed IHC for Tsc2 to confirm efficient gene deletion (Fig 1G). Tsc2 was ubiquitously expressed in the cytoplasm of both germ and somatic cell components of control testis, while in $Tsc2^{F/F}$ *Stra8-Cre* testis, Tsc2 appeared entirely absent from germ cells but retained in Sertoli and interstitial cells. Subsequently, however, we noticed that a fraction of spermatogonia adjacent to the tubule basement membrane still expressed Tsc2, consistent with the fact that *Stra8-Cre* is inactive in some SPCs [12]. Importantly, immunostaining for P-RPS6 indicated robust activation of the mTORC1 pathway in germ cells at different stages of maturation in $Tsc2^{F/F}$ *Stra8-Cre* testis when compared to controls (Fig 1H). *Tsc2* depletion in the testis was also associated with increased phospho-4EBP1 levels (unpublished observations). Thus, *Tsc2* is an important negative regulator of mTORC1 in male germ cells but appears dispensable for the spermatogenic process.

Given that aberrant activation of mTORC1 in SPCs is proposed to be detrimental to their function [6], we analyzed cohorts of $Tsc2^{F/F}$ *Stra8-Cre* adults for defects in germline maintenance and function. As the testes of young $Tsc2^{F/F}$ *Stra8-Cre* adults (1–2 months postnatal) did not display any consistent or obvious phenotype when compared to controls (unpublished observations), we analyzed older (6 months postnatal) animals. However, even at this age, sections of hematoxylin and eosin (H&E)-stained $Tsc2^{F/F}$ *Stra8-Cre* testes appeared similar to controls and comparable numbers of mature spermatozoa were found in the epididymides (Fig 2A). Furthermore, there was no significant change in the number of cells expressing the SPC marker Plzf in sections of $Tsc2^{F/F}$ *Stra8-Cre* testes compared to controls (Fig 2B and Table 1). We conclude that the hyperactivation of mTORC1 in response to *Stra8-Cre*-mediated deletion of *Tsc2* does not result in germline maintenance defects.

SPCs from $Tsc2^{F/F}$ Stra8-Cre testis display larger cell size

Conditional deletion of *Tsc2* with *Stra8-Cre* did not result in a gross testis phenotype; however, some spermatogonia still expressed *Tsc2* in this model. As a subset of SPCs does not express *Stra8-Cre* [12,27], we next analyzed in detail SPC status from $Tsc2^{F/F}$ *Stra8-Cre* testis and the efficiency of *Tsc2* deletion within this cell population. Fixed and permeabilized testis cells from pre-pubertal (2 weeks postnatal) mice were stained for Plzf, c-Kit and Tsc2 and analyzed by flow cytometry; allowing identification of the Plzf-expressing cell pool (Fig 2C). A minor fraction of $Plzf^{pos}$ cells also express c-Kit and represent differentiating SPCs [6,12]. However, there was no significant difference in the fraction of $Plzf^{pos}$ cells that expressed c-Kit in control and $Tsc2^{F/F}$ *Stra8-Cre* testis (Fig 2D), suggesting that the balance between SPC differentiation and self-renewal was not perturbed. Accordingly, the percentage of SPCs within the testis cell populations from $Tsc2^{F/F}$ *Stra8-Cre* and control mice was comparable (Fig 2E).

Importantly, we noticed that the physical size of SPCs from $Tsc2^{F/F}$ *Stra8-Cre* testis, as measured by forward scatter (FSC), was significantly larger than that of control SPCs (Fig 2F). Increased cell size and growth are a hallmark of elevated mTORC1 activity [6,28], further indicating that while SPC status was not perturbed in $Tsc2^{F/F}$ *Stra8-Cre* testis, *Tsc2* deletion should have occurred to some extent. To confirm whether this was indeed the case, we compared Tsc2 protein levels in $Plzf^{pos}$ testis cells by flow cytometry (Fig 2G). Interestingly, essentially all the Plzf-expressing cells from control testis were positive for Tsc2, in agreement with the ubiquitous expression pattern of Tsc2 observed from IHC analysis of testis sections (see above). However, on average, ~40% of SPCs ($Plzf^{pos}$ c-Kit^{neg}) and ~60% of cells at early differentiation stages ($Plzf^{pos}$ c-Kit^{pos}) from $Tsc2^{F/F}$ *Stra8-Cre* testis had lost *Tsc2* expression (Fig 2G and H). That the differentiating SPC population is found to contain more *Tsc2*-ablated cells than the undifferentiated pool suggests that *Stra8-Cre* is most active in differentiating cells and/or in SPCs primed for differentiation, consistent with previous data (see below) [12]. In addition, we confirmed that both mTOR itself and the key downstream target 4EBP1 are ubiquitously expressed within the Plzf-positive pool of juvenile testis, indicating that all SPCs would have the capacity to activate the pathway upon *Tsc2* deletion (Supplementary Fig S2).

Male adult germline maintenance is Tsc2 dependent

Conditional deletion of *Tsc2* in a subset of SPCs primed for differentiation using *Stra8-Cre* did not result in any apparent phenotype. To assess the effect of more extensive *Tsc2* deletion within the SPC pool, we therefore crossed *Tsc2* floxed mice with transgenic animals expressing *Cre* from the *Vasa* promoter. *Vasa-Cre* is induced in embryonic gonocytes prior to formation of the SPC pool and can drive efficient floxed gene deletion within the germline [12,29]. Importantly, from the analysis of pre-pubertal (2 weeks postnatal) testis sections, no gross germ cell phenotype was evident, suggesting that postnatal germline development of $Tsc2^{F/\Delta}$ *Vasa-Cre* mice was unaffected (Supplementary Fig S3A). In addition, the presence of Plzf-expressing cells on the seminiferous tubule basement membrane of juvenile $Tsc2^{F/\Delta}$ *Vasa-Cre* testis indicated that SPC populations were successfully established (Fig 3A). Immunostaining for P-RPS6 did, however, indicate a striking increase in mTORC1 pathway activity in germ cells of juvenile $Tsc2^{F/\Delta}$ *Vasa-Cre* testis and a corresponding loss of *Tsc2* expression (Fig 3B).

Having confirmed that induction of *Tsc2* deletion with a *Cre* transgene that is active from embryonic germ cell stages did not appear to disrupt postnatal testis development and generation of SPCs, we next examined $Tsc2^{F/\Delta}$ *Vasa-Cre* adults for potential testis phenotypes. Strikingly, we found that by 2 months postnatal, the testis of $Tsc2^{F/\Delta}$ *Vasa-Cre* mice contained a significant number of degenerating tubules that had lost or were in the processing of losing germ cell components (Fig 3C and D). This germline degeneration correlated with reduced testis weight of $Tsc2^{F/\Delta}$ *Vasa-Cre*

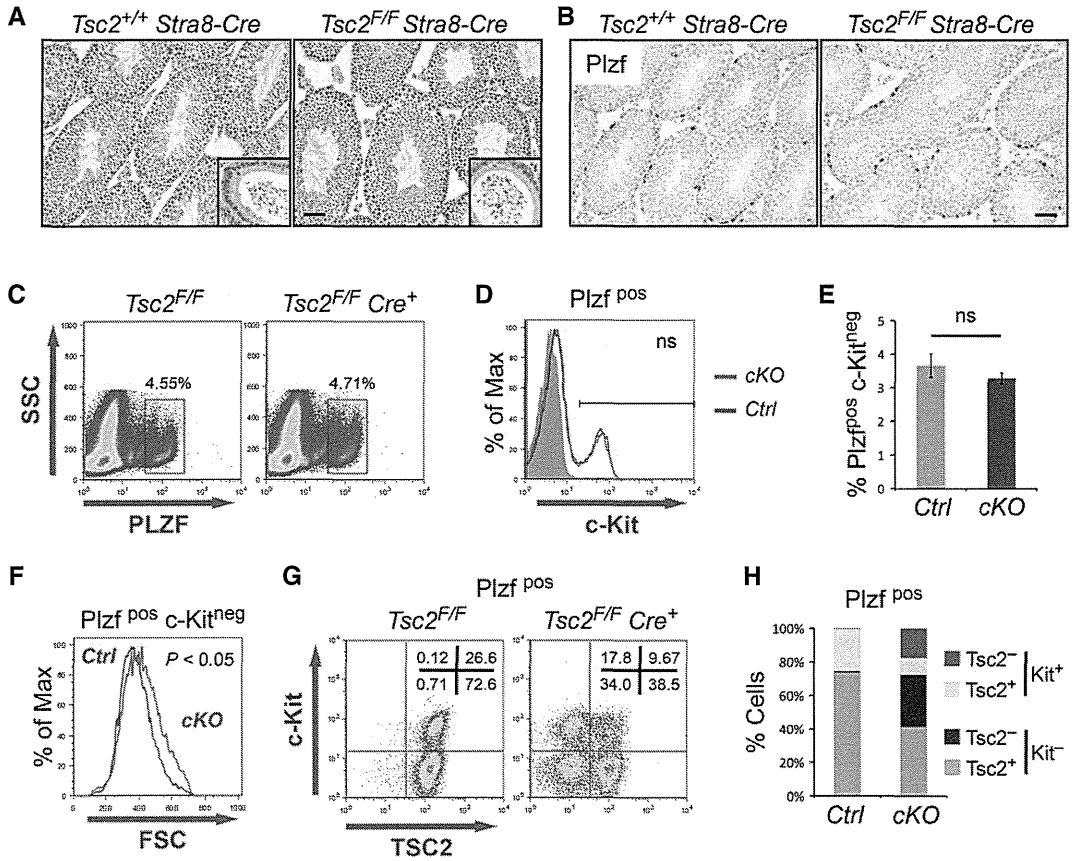

Figure 2. Assessment of SPC status in *Tsc2$^{F/F}$ Stra8-Cre* testis.

A Representative images of testis sections from 6 months postnatal mice of the indicated genotypes stained with hematoxylin and eosin (H&E). Insets show higher magnification details of mature sperm present in the epididymis. Scale bar is 50 μm.

B Representative IHC for Plzf on testis sections as in (A).

C Representative flow cytometric analysis of fixed and permeabilized testis cells from 2 weeks postnatal mice for Plzf expression.

D Analysis of c-Kit expression by the Plzf-positive fractions of control (Ctrl; *Tsc2$^{F/F}$*) and conditional knockout (cKO; *Tsc2$^{F/F}$ Stra8-Cre*) testis cells. Filled histogram (gray) indicates isotype-stained control. No significant difference was found in the percentage of Plzf-positive cells expressing c-Kit between six control and five cKO animals.

E Fraction of total testis cells identified as SPCs (Plzf positive, c-Kit negative) from the flow cytometric analysis of (D). Mean values are shown ± SEM.

F Analysis of cell size by flow cytometry. Representative overlay of forward scatter (FSC) plots of the SPC fractions from 2 weeks postnatal littermate mice. The mean FSC of *Tsc2$^{F/F}$ Stra8-Cre* (cKO) SPCs is significantly increased compared to *Tsc2$^{F/F}$* (Ctrl) cells. Duplicate mice were analyzed per genotype and *P*-value is indicated.

G Representative flow cytometric analysis of Tsc2 and c-Kit expression by the Plzf-positive testis cell population from 2 weeks postnatal mice of the indicated *Tsc2; Stra8-Cre* genotypes. Percentage of cells within each quadrant gate is indicated.

H Quantification of the flow cytometry analysis shown in (G). Mean percentage of Plzf-positive testis cells with indicated Tsc2 and c-Kit expression status is shown. A total of six *Tsc2$^{F/F}$* (Ctrl) and 5 *Tsc2$^{F/F}$ Stra8-Cre* (cKO) animals were analyzed.

adults compared to controls (Fig 3E). Critically, many tubules of adult *Tsc2$^{F/Δ}$ Vasa-Cre* testis, while sometimes still containing spermatocytes and/or spermatids, lacked cells expressing SPC markers including Plzf and Lin28a (Fig 3F) [6,24,30]. This significant and substantial reduction in the number of Plzf-positive cells in adult *Tsc2$^{F/Δ}$ Vasa-Cre* testis indicates an SPC maintenance defect (Table 1), consistent with the observed deterioration of germ cell components. Additionally, mRNA levels of the GDNF receptor components *Gfra1* and *Ret*, critical for SPC maintenance and highly enriched within self-renewing SPC populations, were significantly decreased in *Tsc2$^{F/Δ}$ Vasa-Cre* versus control adult testis (Fig 3G) [8,31,32]. Together, these data indicate that *Tsc2* deletion driven by the *Vasa-Cre* transgene results in an SPC maintenance defect and accompanying germline degeneration.

Tsc2/mTORC1 controls self-renewal versus differentiation fates of SPCs

In contrast to *Stra8-Cre*-mediated *Tsc2* deletion, use of *Vasa-Cre* to drive conditional knockout of *Tsc2* results in depletion of the SPC pool. To better understand why these two models give distinct phenotypes, we next performed a detailed analysis of SPC status in pre-pubertal *Tsc2$^{F/Δ}$ Vasa-Cre* testis in a comparable manner to our assessment of SPC activity in the *Tsc2$^{F/F}$ Stra8-Cre* model (see above). Importantly, flow cytometric analysis of fixed, permeabilized and immunostained cells from *Tsc2$^{F/Δ}$ Vasa-Cre* testis (2 weeks postnatal) revealed a reduction in the Plzf^{pos} population compared to controls (Fig 4A). Importantly, the fraction of Plzf^{pos} cells that co-expressed the differentiation marker c-Kit was significantly

Table 1. Effects of conditional *Tsc2* deletion on the Plzf-expressing spermatogonial pool.

	Plzf ^{pos} cells/tubule cross-section[a]		
Cre driver	Control[b]	*Tsc2* cKO[c]	*P*-value
Stra8-Cre[d]	2.35 ± 0.19	2.15 ± 0.26	0.57
Vasa-Cre[e]	2.10 ± 0.15	0.68 ± 0.05	9.4 9 10^{-5}
Amh-Cre[e]	2.24 ± 0.14	2.09 ± 0.22	0.59

[a]Mean values are shown ± SEM. Three mice per genotype were analyzed for *Stra8-Cre* and *Amh-Cre* cohorts, and four mice per genotype were analyzed for the *Vasa-Cre* group. Over 50 tubule cross-sections were scored per animal.
[b]Littermate controls were of the following genotypes: +/+ *Cre*+ or +/*F Cre*+ for *Stra8-Cre* cohort; +/*F Cre*+ for *Vasa-Cre* and *Amh-Cre* cohorts.
[c]Conditional knockout (cKO) genotypes were *F/F Cre*+ with *Stra8-Cre* and *Amh-Cre* drivers and *F/*Δ *Cre*+ with *Vasa-Cre* driver.
[d]Six months postnatal.
[e]Two months postnatal.

increased in $Tsc2^{F/\Delta}$ *Vasa-Cre* versus control testis, suggesting that SPCs from this knockout model have an aberrant tendency to differentiate and/or reduction in self-renewal (Fig 4B and C). Indeed, the relative fraction of SPCs was significantly reduced in juvenile $Tsc2^{F/\Delta}$ *Vasa-Cre* testis (Fig 4D), demonstrating that *Vasa-Cre*-mediated *Tsc2* deletion is detrimental to the SPC population.

Consistent with successful *Tsc2* ablation, SPCs from pre-pubertal $Tsc2^{F/\Delta}$ *Vasa-Cre* mice demonstrated significant increases in cell size as measured by FSC, an indicator of increased mTORC1 activity (Fig 4E, see above). Critically, when assessing Tsc2 protein levels by flow cytometry, we observed a complete ablation of *Tsc2* expression within the Plzf^{pos} population, irrespective of c-Kit expression, from $Tsc2^{F/\Delta}$ *Vasa-Cre* testis (Fig 4F and G). Together, these data indicate that complete loss of *Tsc2* expression throughout the SPC pool disrupts self-renewal and leads to SPC exhaustion in adults.

To confirm that the effects of *Tsc2* ablation on SPCs are dependent on increased mTORC1 activation, we next tested whether treatment of juvenile $Tsc2^{F/\Delta}$ *Vasa-Cre* mice with the mTORC1 inhibitor rapamycin could rescue the changes in SPC function. Strikingly, upon rapamycin treatment, the fraction of Plzf^{pos} testis cells from $Tsc2^{F/\Delta}$ *Vasa-Cre* mice that expressed c-Kit was now comparable to vehicle-treated controls (Fig 4H and I). The significant increase in percentage of Plzf^{pos} testis cells expressing c-Kit previously detected in $Tsc2^{F/\Delta}$ *Vasa-Cre* versus control mice was still apparent in vehicle-treated animals (Fig 4I; Supplementary Fig S3B). Thus, rapamycin rescues the disrupted balance between self-renewal and differentiation commitment of $Tsc2^{F/\Delta}$ *Vasa-Cre* SPCs. Importantly, this regimen of rapamycin treatment was able to normalize both the fraction of SPCs found within $Tsc2^{F/\Delta}$ *Vasa-Cre* testis cells when compared to vehicle-treated controls and the increased cell size of $Tsc2^{F/\Delta}$ *Vasa-Cre* SPCs (Fig 4I; Supplementary Fig S3C). We conclude that the detrimental effects of *Vasa-Cre*-dependent *Tsc2* deletion on SPC function are mediated through aberrant activation of the mTORC1 pathway.

Transient cell non-autonomous SPC regulation by Tsc2/mTORC1 in the niche

It has recently become apparent that stem cell behavior can be affected in a cell non-autonomous manner by the level of mTORC1 activity within cells contributing to the stem cell niche. In particular, mTORC1-dependent changes in production of paracrine factors by niche cells have been described to impact both positively and negatively on stem cell self-renewal in other systems [33,34]. While the contribution of different somatic cell types to the SPC niche remains an area of intense study, the Sertoli cell is understood to be a critical component through its production of growth factors required for SPC self-renewal and growth [5]. In wild-type adult testis, we find evidence of stage-specific mTORC1 activation in Sertoli cells suggesting a potential role for this pathway in niche function (Fig 1A, see above).

Thus, we next assessed the indirect niche-dependent effects of aberrant mTORC1 activation on SPC function. To this end, *Tsc2* floxed mice were crossed with animals carrying the *Amh-Cre* transgene, which express *Cre* in a Sertoli cell-specific fashion from the anti-Mullerian hormone (*Amh*) promoter [35]. *Amh-Cre* expression is detectable by embryonic day (E) 11.5 in the developing testis [36]. Analysis of juvenile (3 weeks postnatal) $Tsc2^{F/F}$ *Amh-Cre* testis revealed an apparent disruption of the seminiferous epithelium compared to controls, the lumen of some tubules appearing full of the eosinophilic cytoplasm from hypertrophic Sertoli cells (Supplementary Fig S4A). Meiotic cell degeneration and vacuolization could also be observed in these tubules (Supplementary Fig S4A and unpublished observations), consistent with a previous study [37]. However, these changes in tubule morphology were temporary, and in young $Tsc2^{F/F}$ *Amh-Cre* adults (2 months postnatal), the testis histology appeared grossly normal compared to controls (Supplementary Fig S4B).

Immunostaining testis sections of young $Tsc2^{F/F}$ *Amh-Cre* adults for the Sertoli cell marker Sox9 identified a typical population of Sertoli cells localized to the basal layer of the seminiferous tubules (Fig 5A) [38]. As anticipated, Sertoli cells of adults displayed striking increases in staining for P-RPS6, confirming successful deletion of *Tsc2* in this cell population (Fig 5B). Importantly, however, numbers of Plzf-positive spermatogonia from adult $Tsc2^{F/F}$ *Amh-Cre* testis (2 months postnatal) were comparable to controls, indicating that SPC activity was unaffected by aberrant mTORC1 activation in Sertoli cells (Fig 5C and Table 1).

Although the Plzf^{pos} spermatogonial population appeared unaffected in young $Tsc2^{F/F}$ *Amh-Cre* adults, we next assessed SPC status in a more detailed fashion in juvenile mice by flow cytometric analysis of fixed and permeabilized testis cells (see above). Immunostaining for the SPC marker Plzf together with the Sertoli cell marker Sox9 demonstrated minor, yet significant, alterations in the relative proportions of these cell types within the pre-pubertal testis (Fig 5D and E). An observed decrease in the fraction of Sox9^{pos} Sertoli cells from $Tsc2^{F/F}$ *Amh-Cre* testis could also be inferred from decreased expression of the Sertoli cell-expressed gene *Amh* as detected by RT–PCR of testis RNA (Supplementary Fig S4C) [39]. Critically, however, the percentage of Plzf^{pos} cells from $Tsc2^{F/F}$ *Amh-Cre* testis that expressed c-Kit was comparable to that of control testis, indicating that self-renewal versus differentiation decisions of SPCs was not substantially affected (Fig 5F and G). Indeed, expression of glial cell line-derived neurotrophic factor (GDNF), a key Sertoli cell-derived factor that drives SPC self-renewal, was not significantly altered in $Tsc2^{F/F}$ *Amh-Cre* testis compared to controls (Supplementary Fig S4C). Together, these data suggest that while some relative expansion of the Plzf^{pos} cell

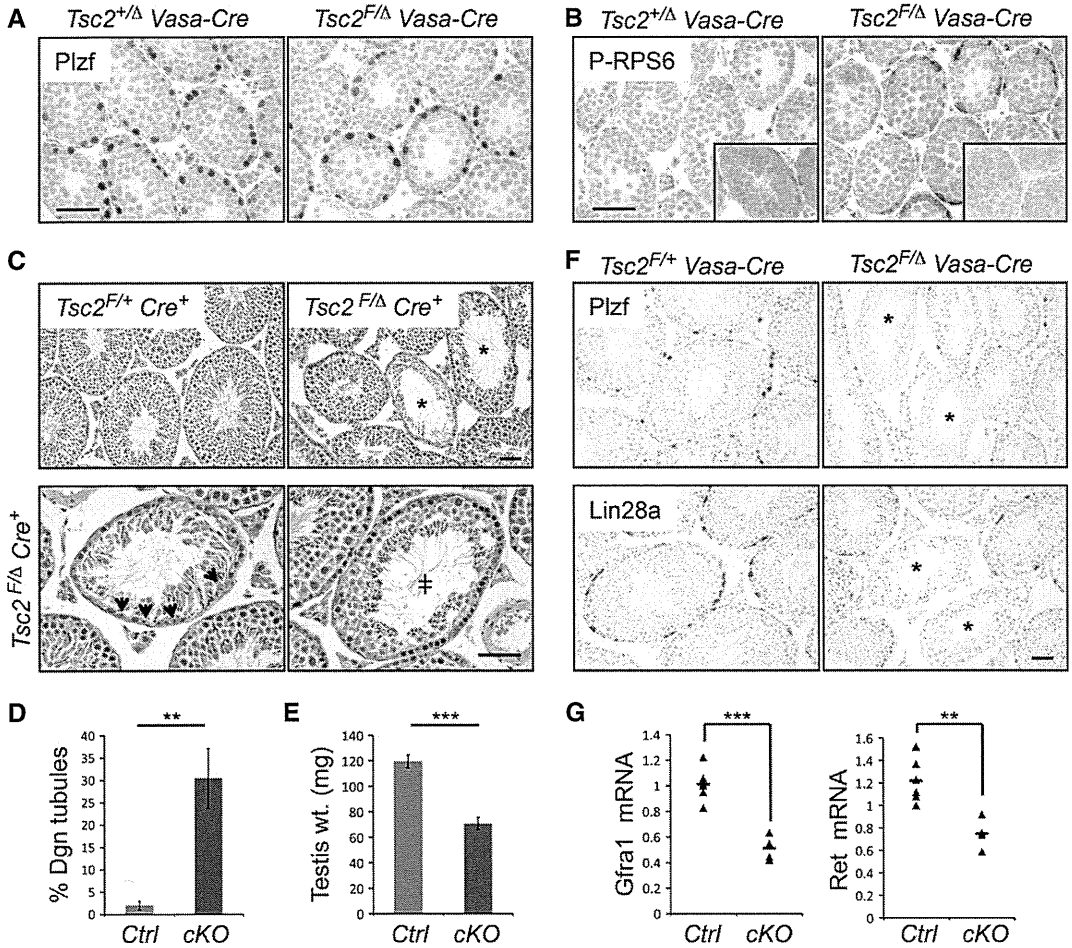

Figure 3. *Vasa-Cre*-mediated *Tsc2* deletion in germ cells drives SPC exhaustion.

A Representative IHC for Plzf on testis sections from 2 weeks postnatal mice. Scale bar: 50 μm.

B IHC for P-RPS6 on testis sections from 2 weeks postnatal mice. Insets show corresponding IHC for Tsc2. Scale bar: 50 μm.

C H&E-stained sections of testis from 2 months postnatal mice of the indicated *Tsc2; Vasa-Cre* genotypes. Asterisks indicate degenerating tubules displaying substantial germ cell loss. Lower panels show examples of degenerating tubules from a $Tsc2^{F/\Delta}$ *Vasa-Cre* adult at higher magnification. Arrowheads indicate Sertoli cells in a tubule containing maturing spermatozoa but lacking preceding germ cell stages. Tubules at initial stages of degeneration with some remaining germ cell components are indicated (♯). Scale bar: 50 μm.

D Quantification of the percentage of degenerating (Dgn) seminiferous tubules displaying germ cell loss from 2 months postnatal $Tsc2^{F/+}$ *Vasa-Cre* (Ctrl) and $Tsc2^{F/\Delta}$ *Vasa-Cre* (cKO) mice. Tubules were scored from H&E-stained sections as indicated in (C). Four mice were analyzed per genotype and over 70 tubule cross-sections were scored per animal. Graph indicates mean values ± SEM. $^{**}P < 0.01$.

E Testis weights of 2 months postnatal $Tsc2^{F/+}$ *Vasa-Cre* (Ctrl) and $Tsc2^{F/\Delta}$ *Vasa-Cre* (cKO) mice. A total of four control and 2 cKO mice were analyzed. Mean value is shown ± SEM. $^{***}P < 0.001$.

F IHC for Plzf (top panels) and Lin28a (bottom panels) on testis sections from 2 months postnatal mice of the indicated genotypes. Asterisks indicate tubules lacking Plzf- or Lin28a-expressing cells. Scale bar: 50 μm.

G Quantitative RT–PCR for GDNF receptor components from total testis cells of 2 months postnatal $Tsc2^{F/+}$ *Vasa-Cre* (Ctrl) and $Tsc2^{F/\Delta}$ *Vasa-Cre* (cKO) mice. mRNA levels are corrected to those of β-actin and normalized to a control sample. Testes from four controls and two cKO mice were analyzed. Horizontal bars indicate mean values. $^{**}P < 0.01$; $^{***}P < 0.001$.

pool occurs in the pre-pubertal testis in response to aberrant mTORC1 activation in Sertoli cells, SPC fate and the SPC population of young adults are both unaffected.

Stra8-Cre preferentially marks mTORC1 active committed progenitors

Through efficient *Vasa-Cre*-mediated deletion of *Tsc2* in SPCs, we have confirmed that aberrant mTORC1 activation in SPCs promotes differentiation commitment and results in germline degeneration [6]. In contrast, *Stra8-Cre*-driven *Tsc2* deletion within a subset of SPCs has no apparent functional consequences. Given that *Stra8* itself is associated with germ cell differentiation [40], we considered that the *Stra8-Cre* transgene might exhibit selective expression in differentiation-committed SPCs. Deleting *Tsc2* in those SPCs that already show evidence of mTORC1 activation (see above) and that make limited contributions to steady-state germline maintenance can explain the lack of phenotype in $Tsc2^{F/F}$ *Stra8-Cre* animals.

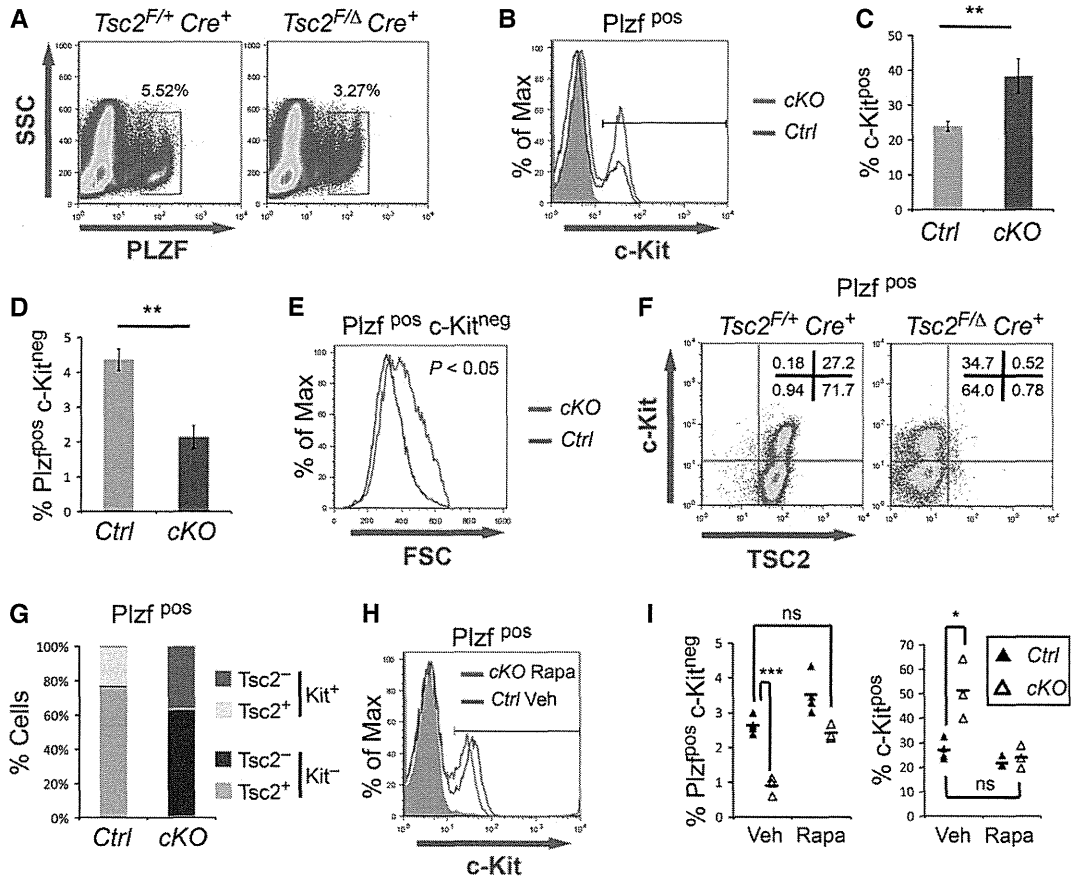

Figure 4. Analysis of SPC status in *Tsc2$^{F/\Delta}$ Vasa-Cre* testis.

A Flow cytometric analysis of testis cells from 2-week postnatal mice of the indicated *Tsc2; Vasa-Cre* genotypes. Percentage of Plzf-positive cells is shown.

B Analysis of c-Kit expression by the Plzf-positive testis cells of control (Ctrl; *Tsc2$^{F/+}$ Vasa-Cre*) and conditional knockout (cKO; *Tsc2$^{F/\Delta}$ Vasa-Cre*) mice from A. Filled histogram (gray) indicates isotype control.

C Testis cells from 2-week postnatal control and cKO mice were analyzed by flow cytometry as in A and B. Graph indicates percentage of Plzf-positive cells expressing c-Kit. Mean values are shown ± SEM. A total of six control and four cKO animals were analyzed. $^{**}P < 0.01$.

D Percentage of SPCs (Plzf positive, c-Kit negative) within the testis cell populations from C. Mean values are shown ± SEM. $^{**}P < 0.01$.

E FSC plot overlays of the SPC fractions from 2-week postnatal littermate mice. The mean FSC of *Tsc2$^{F/\Delta}$ Vasa-Cre* (cKO) SPCs is significantly increased compared to control SPCs (*Tsc2$^{F/+}$ Vasa-Cre* or *Tsc2$^{\Delta/+}$ Vasa-Cre*). A total of four control and two cKO mice were analyzed and *P* value is indicated.

F Flow cytometric analysis of Tsc2 and c-Kit expression by Plzf-positive testis cells from 2-week postnatal mice. Percentage of cells within gates is indicated.

G Quantification of analysis in F. Graph shows mean percentage of Plzf-positive cells with the indicated Tsc2 and c-Kit expression. A total of six control (*Tsc2$^{F/+}$ Vasa-Cre* or *Tsc2$^{\Delta/+}$ Vasa-Cre*) and 4 *Tsc2$^{F/\Delta}$ Vasa-Cre* (cKO) animals were analyzed.

H Flow cytometric analysis of c-Kit expression by Plzf-positive testis cells from vehicle (Veh)-treated control (*Tsc2$^{F/+}$ Vasa-Cre*) and rapamycin (Rapa)-treated *Tsc2$^{F/\Delta}$ Vasa-Cre* (cKO) juvenile mice.

I Testis cells from Veh- and Rapa-treated control (*Tsc2$^{F/+}$ Vasa-Cre* or *Tsc2$^{\Delta/+}$ Vasa-Cre*) and cKO juvenile mice were analyzed by intracellular staining and flow cytometry as in H. The fraction of testis cells identified as SPCs (Plzf positive, c-Kit negative) is indicated in the left panel, while the percentage of Plzf-positive cells expressing c-Kit is on the right. A total of four control and three cKO mice were analyzed for each treatment group. Horizontal bars indicate mean values and selected *P* values are included. $^{*}P < 0.05$; $^{***}P < 0.001$.

To test whether *Stra8-Cre* is expressed in discrete subsets of SPCs as predicted, we crossed *Stra8-Cre* mice with transgenic *Z/EG* reporter animals that express enhanced green fluorescent protein (GFP) upon Cre-dependent deletion of an upstream βgeo cassette [12,41]. Importantly, from whole-mount analysis of adult and prepubertal *Z/EG; Stra8-Cre* testis, we confirmed that a fraction of Plzf-positive SPCs was GFP negative, thus indicating that they neither expressed *Cre* nor were derived from *Cre*-expressing cells (Supplementary Fig S5A). Correspondingly, analysis of juvenile *Z/EG; Stra8-Cre* testis by flow cytometry demonstrated that while a majority of SPCs were GFP positive, a discrete GFP-negative population was observed (Fig 6A). In addition, cells initiating differentiation (Plzf^{pos} c-Kit^{pos}) were largely GFP^{pos}, consistent with previous data and the pattern of *Tsc2* deletion in *Tsc2$^{F/F}$ Stra8-Cre* testis (see above) [12].

Strikingly, the cell size of GFP^{pos} (Stra8-Cre^{pos}) SPCs, as measured by FSC, was significantly increased compared to that of GFP^{neg} (Stra8-Cre^{neg}) SPCs from *Z/EG; Stra8-Cre* testis (Fig 6B and C). Further, the size of cells initiating differentiation (Plzf^{pos} c-Kit^{pos}) was significantly increased above both SPC fractions. Importantly,

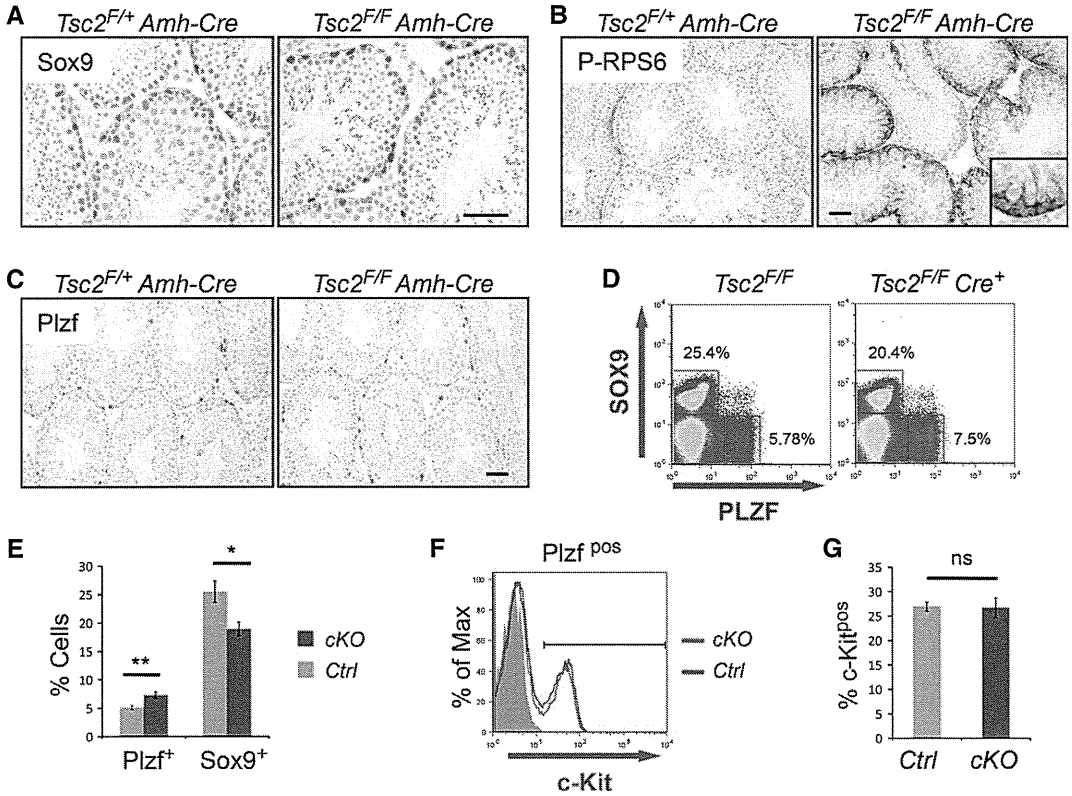

Figure 5. *Tsc2*-deficient Sertoli cells support SPC function.

A IHC for the Sertoli cell marker Sox9 on testis sections from 2 months postnatal mice of the indicated genotypes. Scale bar: 50 μm.

B IHC for P-RPS6 on testis sections from 2 months postnatal mice. Scale bar: 50 μm.

C IHC for Plzf on testis sections from 2 months postnatal mice. Scale bar: 50 μm.

D Representative flow cytometric analysis of Sox9 and Plzf expression by testis cells from 2 weeks postnatal mice of the indicated *Tsc2; Amh-Cre* genotypes. Plzf- and Sox9-positive cell populations are indicated.

E Testis cells from 2 weeks postnatal control (*Tsc2*$^{F/+}$ or *Tsc2*$^{F/F}$) and cKO (*Tsc2*$^{F/F}$ *Amh-Cre*) mice were analyzed for Plzf and Sox9 expression by flow cytometry as described in (D). Graph indicates the mean percentage of testis cells positive for Plzf and Sox9 ± SEM. Five mice were analyzed per genotype group. *$P < 0.05$; **$P < 0.01$.

F Comparative flow cytometry analysis of c-Kit expression by Plzf-positive testis cells from control (*Tsc2*$^{F/F}$) and *Tsc2*$^{F/F}$ *Amh-Cre* (cKO) 2 weeks postnatal mice. Filled histogram (gray) indicates isotype-stained control.

G Percentage of Plzf-positive cells from the flow cytometric analysis described in (E) that express c-Kit. Mean values are shown ± SEM.

inhibition of mTORC1 *in vivo* by rapamycin treatment of *Z/EG; Stra8-Cre* juvenile mice essentially eliminated differences in cell size between the cell fractions, confirming that size changes are mediated by differential mTORC1 activation (Fig 6B). These results indicated that mTORC1 activity increases in a graded fashion from Stra8-Cre^{neg} SPCs (low) to Stra8-Cre^{pos} SPCs (intermediate) to cells initiating differentiation (high) and suggested a positive correlation between *Stra8-Cre* expression, mTORC1 activation and SPC differentiation. That *Stra8-Cre* was preferentially expressed in mTORC1-active SPC populations was further suggested by whole-mount analysis of juvenile and adult *Z/EG; Stra8-Cre* seminiferous tubules (Fig 6D). The majority of mTORC1-active A_{al} subsets were GFP positive, while GFP-negative Plzf-positive cells were typically A_s and A_{pr} and P-4EBP negative/low.

Together, our data indicated that within the SPC pool *Stra8-Cre* is predominantly expressed by differentiation-committed cells that have increased mTORC1 activity (see above). To further define this expression pattern, we compared GFP expression in self-renewing and committed SPC fractions of *Z/EG; Stra8-Cre* testis, taking advantage of selective markers for these populations. Interestingly, within the Gfrα1-positive self-renewing SPC subpopulation of both juvenile and adult *Z/EG; Stra8-Cre* mice, GFP expression was markedly heterogeneous (Fig 6E; Supplementary Fig S5B). Accordingly, more than 20% of Gfrα1-positive cells were GFP negative in the juvenile, demonstrating that the transgene was inactive in a substantial fraction of the self-renewing SPC pool (Fig 6F). Conversely, expression of retinoic acid receptor γ (RARγ), a marker specific for differentiation-prone A_{al} SPCs and spermatogonia at the very first step of the differentiation pathway (A_1 cells), correlated strongly with GFP expression (Fig 6E; Supplementary Fig S5C) [42]. Specifically, only approximately 5% of RARγ-positive cells in the juvenile testis were GFP negative (Fig 6F). This substantial difference in Cre activity between the Gfrα1 and RARγ populations confirms that *Stra8-Cre* is preferentially active in committed progenitors although is still evident within a portion of the self-renewing pool. Considering that recombination of both floxed *Tsc2* alleles in a cell would probably

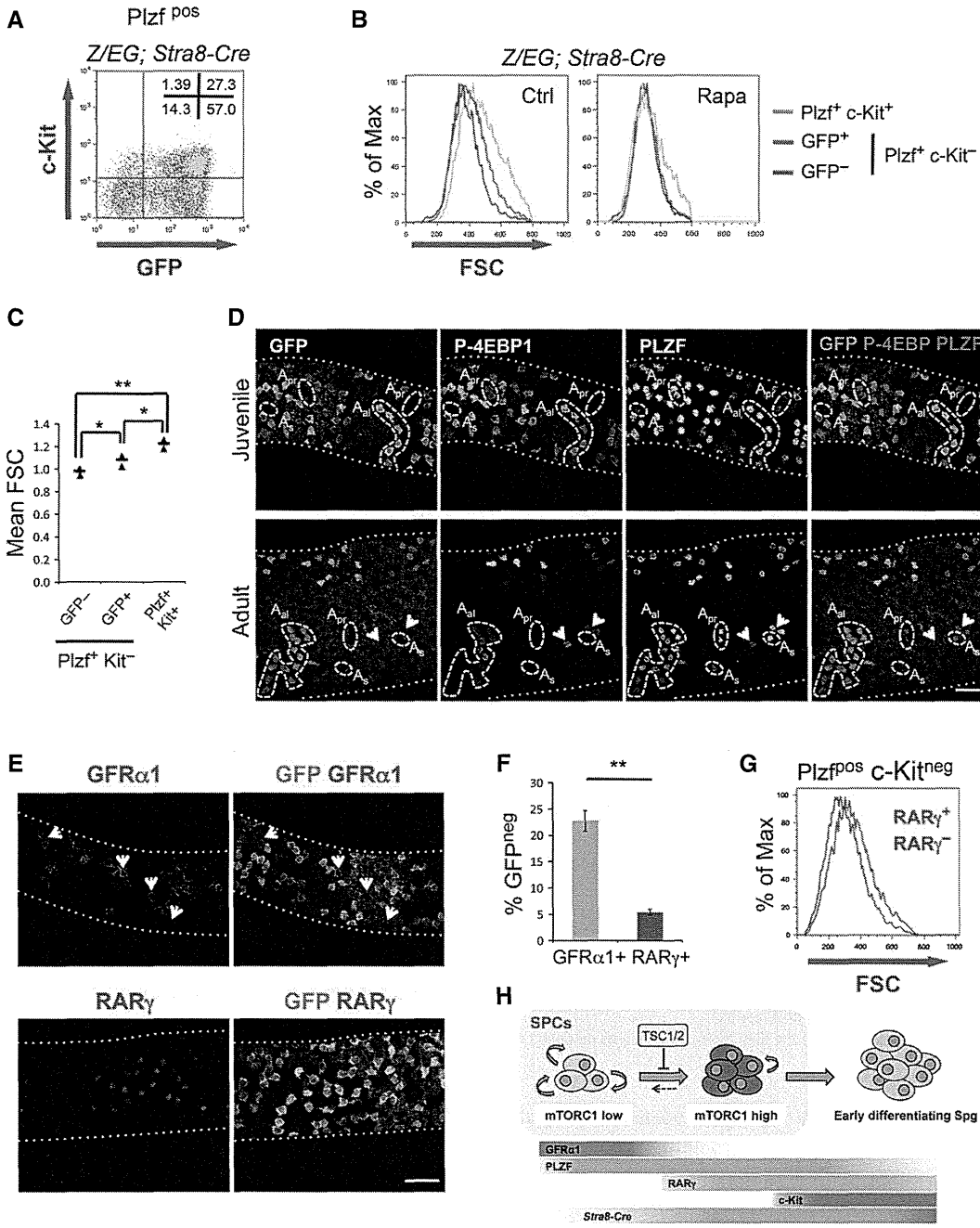

Figure 6.

be less efficient than recombination of a single *ZEG* reporter, we conclude that *Stra8-Cre*-driven *Tsc2* deletion would be inefficient within the self-renewing SPC pool but significant within mTORC1-active committed progenitors.

We note that in the absence of appropriate antibodies to other committed SPC markers such as Ngn3, expression of RARγ effectively labels those SPCs and spermatogonia at the earliest stages of differentiation commitment (Supplementary Fig S5D). Moreover, RARγ^{pos} SPCs are significantly larger than RARγ^{neg} SPCs, indicating that RARγ expression successfully marks mTORC1-active, differentiation-committed cells (Fig 6G; Supplementary Fig S5E).

Role of the mTORC1 pathway in defining SPC heterogeneity and fate

The SPC population can be envisaged as being composed of discrete cell subsets, distinguishable by morphology and gene expression, which exhibit varying propensities for self-renewal and differentiation (Fig 6H). Our data demonstrate that SPC subsets with high self-renewal potential suppress mTORC1 activity, while those populations with high differentiation tendencies have an activated mTORC1 pathway. Given that we find aberrant mTORC1 activation to inhibit SPC self-renewal, we propose that differential